



**STIMULATED BRILLOUIN SCATTERING BEAM CLEANUP AND
BEAM PHASING THROUGH TWO PASSIVE CHANNELS**

THESIS

Omar Gamboa, Second Lieutenant, USAF

AFIT/GAP/ENP/07-03

**DEPARTMENT OF THE AIR FORCE
AIR UNIVERSITY**

AIR FORCE INSTITUTE OF TECHNOLOGY

Wright-Patterson Air Force Base, Ohio

APPROVED FOR PUBLIC RELEASE; DISTRIBUTION UNLIMITED

The views expressed in this thesis are those of the author and do not reflect the official policy or position of the United States Air Force, Department of Defense, or the United States Government.

AFIT/GAP/ENP/07-03

STIMULATED BRILLOUIN SCATTERING BEAM CLEANUP
AND BEAM PHASING THROUGH TWO PASSIVE
CHANNELS

THESIS

Presented to the Faculty

Department of Engineering Physics

Air Force Institute of Technology

Air University

Air Education and Training Command

In Partial Fulfillment of the Requirements for the

Degree of Master of Science

Omar Gamboa, B.S.

Second Lieutenant, USAF

March 2007

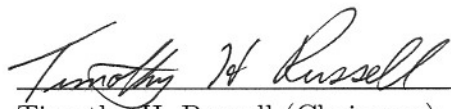
APPROVED FOR PUBLIC RELEASE; DISTRIBUTION UNLIMITED

AFIT/GAP/ENP/07-03

STIMULATED BRILLOUIN SCATTERING BEAM CLEANUP AND
BEAM PHASING THROUGH TWO PASSIVE CHANNELS

Omar Gamboa, B.S.
Second Lieutenant, USAF

Approved:



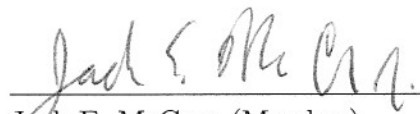
Timothy H. Russell (Chairman)

14 MAR 2007
Date



Thomas G. Alley (Member)

14 Mar 2007
Date



Jack E. McCrae (Member)

15 Mar 2007
Date

Abstract

Stimulated Brillouin scattering (SBS) beam cleanup and SBS piston correction properties are explored. This research measures the beam cleaning and phase-conjugating properties of stimulated Brillouin Scattering in an optical fiber. A single-frequency Nd:YAG NPRO laser source was used operating at $1.06\text{ }\mu\text{m}$ with maximum output of 700mW in a single-mode beam. A diode-pumped Nd:YAG rod is used to amplify the beam giving a total output of $\sim 1.4\text{W}$.

The first stage of this research began by coupling an aberrated beam into a long multimode $62.5\text{ }\mu\text{m}$ core fiber to demonstrate its beam cleanup properties. The Stokes beam obtained was shown to be the fundamental fiber mode, LP_{01} .

The second stage spatially divided the pump beam into two equal halves. Each half was then sent through different channels. The path length of one channel remained fixed while the other path contained a retro-reflector mounted on a piezoelectric movable stage to allow path length variation. The two channels were then tiled next to each other and coupled into a 4.6 km multimode $62.5\text{ }\mu\text{m}$ core fiber. Phasing of the reflected Stokes beam was investigated by observing the interference fringes produced by using a lateral shearing interferometer (LSI). The reflected Stokes beam exhibited a gaussian beam profile. Results from the LSI interference patterns indicate that the two halves of the reflected beam immediately after exiting the fiber were in phase.

The two halves then retraced their respective paths back through their own individual channels and the interference fringes were analyzed using the LSI. By analyzing the Stokes beam after propagating back through the two channel configuration, it was observed that phase conjugation did not occur. This was observed by discontinuity of the fringes across three regions of interference. The fringes were able to be aligned by shifting the movable stage by less than a wavelength.

Acknowledgements

First of all, I want to thank God for the education opportunity that I was given here at AFIT. I wish to thank my advisor Maj Timothy H. Russell for his patience and for his support in the completion of this research. Also I need to recognize the help of LtCol Thomas G. Alley, Maj Massey, Capt Terry and 1Lt Baird for teaching me the techniques of working in the lab and for the group meetings we had each week. Finally, I wish to dedicate this to my loving parents who have always supported me into every decision I have ever made and for making me what I am today. This is for you.

Omar Gamboa

Table of Contents

	Page
Abstract	iv
Acknowledgements	v
List of Figures	viii
I. Introduction	1-1
1.1 Motivation	1-1
1.2 Overview	1-4
1.3 Document Organization	1-5
II. Theoretical Background	2-1
2.1 Nonlinear Optics	2-1
2.2 Stimulated Brillouin Scattering Phenomenon	2-4
2.3 SBS Threshold	2-6
2.4 Optical Phase Conjugation	2-8
2.5 Optical Fibers	2-10
III. SBS Beam Cleanup	3-1
3.1 Background	3-1
3.2 Experiment and Results	3-1
3.3 Conclusion	3-6
IV. Beam Phase Conjugation of Two Passive Channels	4-1
4.1 Background	4-1
4.2 Experiment and Results	4-7
4.3 Conclusion	4-14

	Page
V. Lateral Shearing Interferometer Testing	5-1
5.1 Two Microscope Slides	5-1
5.2 Two Optical Flats	5-3
5.3 Single Optical Flat	5-4
5.4 Two Optical Wedges	5-5
VI. Conclusion and Recommendations for Future Work	6-1
6.1 Conclusion	6-1
6.2 Recommendations	6-2
Bibliography	BIB- 1
Vita	VITA-1

List of Figures

Figure		Page
2.1.	Contrast between (a) a linear function, and (b) a nonlinear function ¹¹	2-2
2.2.	Schematic representation of the stimulated Brillouin scattering process.	2-5
2.3.	Comparison between a mirror and a phase-conjugation mirror.....	2-9
2.4.	Snell's law for a ray going from n_1 to a surface of index n_2	2-11
2.5.	Representation of an optical fiber exhibiting the core, cladding, and buffer/jacket regions..	2-13
2.6.	Propagation of light inside an optical fiber.	2-14
2.7.	Computer generated 2D plot exhibiting the fundamental fiber mode LP ₀₁	2-15
2.8.	Spatial distribution in 3D of the LP ₀₁ mode. Notice that the intensity profile is similar to that of a Gaussian beam.	2-15
3.1.	Experimental setup used to demonstrate the SBS beam cleanup properties of a long multimode fiber.	3-2
3.2.	Input power as a function of the input power.	3-4
3.3.	Stokes power as a function of the input power.	3-4
3.4.	Oscilloscope view showing the data obtain with the Fabry-Perot spectrum analyzer.	3-5
3.5.	Representation of the procedure used to measure the SBS frequency shift.	3-6
3.6.	Beam profile of aberrated beam (left) and the Stokes beam gener- ated before double-passing the aberrator (right).	3-7
4.1.	Optical layout for overlap-coupling experiment developed by Moyer <i>et al.</i> ⁵	4-3
4.2.	Lateral shearing interferometer (LSI) for two semicircles that travel through different channels. The interference produced using the LSI is the diagnostic tool to determine piston error conjugation.	4-4
4.3.	Experimental setup of a short multimode fiber as a PCM by Willis <i>et al.</i> ⁶	4-5
4.4.	Schematic representation of the experimental setup to investigate the SBS phasing properties.	4-8
4.5.	Beam profile before being separated into two channels.	4-9
4.6.	Beam profile after beam goes through separate paths and then rejoined.	4-9
4.7.	Two reflections from LSI.	4-10

Figure	Page
4.8.	Self-interference between the two reflections from the LSI. 4-10
4.9.	Interference showing that the beams are not in phase. 4-11
4.10.	Two reflections from the Stokes beam just after exiting the fiber. Here, the two beam reflections appear to be the fundamental mode LP ₀₁ 4-12
4.11.	3D profile of the two reflections of the Stokes just after exiting the fiber. The beams are now continuous and the division between the beams has dissappeared due to beam cleanup. 4-12
4.12.	Interference pattern showing that the two sides of the beam are phased. The reflections that create this interference come from the two reflections of the Stokes beam immediately after exiting the fiber. 4-13
4.13.	Data from the lateral shearing interferometer showing discontinuity throughout the three regions. 4-14
4.14.	From discontinuity to continuity 4-15
4.15.	LSI data showing no fringes in the mutual interference region due to vibrational disturbance. 4-15
5.1.	Interference pattern obtain from a LSI consisting of two microscope slides as performed by Willis. ⁶ Notice that the boundary regions cannot be easily distinguished 5-1
5.2.	Interference pattern observed when a microscope slide was used to build the LSI. Notice that the boundaries between the regions are difficult to identified as this was the case in previous experiments. . . . 5-2
5.3.	The two reflections of an LSI consisting of two microscope slides. Interference shown here may be developed as the beam is transmit- ted through the amplifier. 5-2
5.4.	Interference pattern between the two optical flats as an LSI. The boundaries are not easily distinguishible. 5-3
5.5.	Interference of two reflections from a single optical flat was used as a LSI. 5-3
5.6.	LSI interference using an optical flat. 5-4
5.7.	LSI built with two wedges. 5-5

STIMULATED BRILLOUIN SCATTERING BEAM CLEANUP AND BEAM PHASING THROUGH TWO PASSIVE CHANNELS

I. Introduction

“Tactical high energy lasers have the capacity to change the face of the battle-field”

US Army Lt Gen Joseph Cosumano

1.1 Motivation

It was in 1917, when Albert Einstein first theorized about the process of stimulated emission, the driving mechanism of today’s lasers.¹ More than 80 years later, the laser has become a powerful tool in the everyday life of our civilization. Lasers are utilized in a wide range of applications, some of which include basic scientific research, test and measurement, industrial processing, microelectronics, biomedicine, environmental science, avionics, entertainment and telecommunications.²

Lasers have been employed by the military as a means of range finding and targeting purposes, but never as a primary weapon. Now in this new era, lasers are stepping into the main stage as the weapons of the future for the 21st century. Weapons like the Mobile Tactical High Energy Laser in development by the US Army, the Advanced Tactical Laser (ATL), and the Airborne Laser (ABL), currently being developed by the US Air Force are paving the way for far more complex weapons in the near future.^{3,4}

Just like in the case of microchips, researchers are looking for ways to reduce the size of current lasers without having to sacrifice power in return. The goal is to have an

efficient, but at the same time, powerful high energy laser. The current approaches taken by the military in the laser programs mentioned before utilize a Chemical Oxygen Iodine Laser (COIL) which can attain power outputs in the megawatt range.⁴ Although effective in achieving enough power for directed energy applications, they present certain disadvantages. One of these comes from the fact that chemical lasers require a large amount of chemicals to generate power. Providing the necessary Cl_2 and H_2O_2 needed for the chemical process gives the ABL a limited amount of times in which the laser can be employed.

An alternative to chemical lasers would be solid-state lasers. Solid-state lasers use a crystalline or glass material doped with an ion. The ions can be pumped using flashlamps or diodes to emit radiation. Compared to the chemical lasers in use by the United States military, solid-state lasers would be more efficient such that it could be conceivable to supply the necessary energy from the engine of an Air Force F-16.³ The disadvantage at this moment is that in terms of power output, solid-state lasers are far from matching chemical lasers.

One approach to increasing the amount of power obtained from solid-state lasers consists on the implementation of what is called a master oscillator power amplifier (MOPA).⁵ MOPA consists of a beam propagating through an amplifying medium, resulting in an increment of the power output. To take advantage of this amplifying system, a second pass configuration system is usually implemented. The amplification in this system is limited by nonlinear effects or even damages in the amplifier that can cause aberrations in the beam output. By using a phase conjugate mirror (PCM) to retro-reflect the beam, it is possible to correct any aberrations imposed by the system. In this case, allowing the beam to propagate through the system several distortions would be induced by the first pass. Implementing the use of a PCM to reverse the beam wavefront would allow for a second pass through the system, such that all of the distortions created by the first pass are corrected.

Because a single amplifier will still produce relatively low power, it is desirable to use multiple amplifiers in parallel for a single master oscillator. The beam can be divided into different channels which are then individually amplified. Unfortunately, as each part travels through its own channel, a phase delay also known as piston error will be produced due to the difference in path length between the channels. Therefore, when the beams are recombined the wavefronts are no longer in phase.

It is possible to compensate for this phase delay between the channels using a phase conjugate mirror (PCM) to induce a second pass through the system. In a multi-channel double pass MOPA each beam travels through its own individual channel. Each channel is amplified separately before reflecting back from a PCM. Because of this double-pass through the MOPA system and the implementation of a PCM, all the channels are phased, thus the phase delay that existed between them was eliminated. In contrast, if a conventional mirror is used to reflect the beams, the phase delay between channels is increased since the beams travel through their individual paths twice without any sort of phase correction. A PCM can be created by inducing Stimulated Brillouin scattering (SBS) in a cell or in an optical fiber, which has been shown to behave as a PCM for short multimode fiber.^{5,6} In addition, SBS phase conjugation was also shown to provide a way to compensate for aberrations in the optical system.⁶ Investigations have shown that the properties of SBS induced in a multimode optical fiber are dependent of length. For long fibers of a few kilometers, the SBS beam generates the fundamental LP_{01} fiber mode regardless of the input beam.^{7,8,9} In the case for short fibers of less than 10m of length, a phase conjugate beam was shown to be generated.⁶

Contradictory evidence was shown by Grime¹⁰ which suggested that when long multimode fiber were used, phasing of two beam paths was possible even when a spatial conjugate of the beam was not produced. To clarify the results, a similar experiment performed by Grime is presented in this research. The major difference consists of observing the characteristics of the beams immediately after exiting the long multimode fiber and after the second pass through the system.

1.2 Overview

The focus of this research consisted of exploring the properties of stimulated Brillouin scattering to understand its properties as a phase conjugating mirror for possible applications in a MOPA configuration. The first stage of this research began by coupling an aberrated beam into a long multimode 62.5 μm core fiber to demonstrate its beam cleanup properties. For SBS beam cleanup, the Stokes beam generates a Gaussian-like beam shown to be the fundamental fiber mode LP_{01} regardless of the beam being coupled into the SBS medium. This cleanup property of the long multimode fiber aids in the understanding of how it may play a vital role in the next part of this research, where two beams are coupled into the fiber.

The second stage of the investigation consisted of spatially dividing the pump beam into two equal halves. Each half was then sent through two channels of different path lengths. The path length of one channel remained fixed while the other path contained a retroreflector mounted on a piezoelectric movable stage to allow path length variation. The output of these two channels were then tiled next to each other and coupled into the long multimode 62.5 μm core fiber. Phasing of the reflected Stokes beam was investigated by observing the interference fringes produced by using a lateral shearing interferometer (LSI) which is explained thoroughly in Chapter 3. The reflected Stokes beam produced a Gaussian-like beam which was later investigated for its phasing properties using the LSI. As each half travels back through its own individual channel of different path length, the interference fringes created by the interference of the beams from both sides were analyzed by employing the LSI once again.

Several significant accomplishments were made in this research and are shown through this document. These are:

1. SBS beam cleanup in a long multimode fiber.
2. SBS beam phasing for a single pass in a two passive channel system.

3. SBS beam phasing disproved for a two channel system over a double pass through the system.

1.3 Document Organization

This document begins with Chapter 2 in which the theoretical background information regarding this research is presented. This is followed by the methodology, setup, results and analysis of two correlated experiments investigated in this thesis. Specifically, Chapter 3 describes the beam cleaning properties of SBS in a long multimode fiber and Chapter 4 the phasing properties of SBS phase conjugation for this medium. Chapter 5 overviews several test results concerning the development of LSI as a device for measuring phase conjugation. Results are then summarized in Chapter 6 and a conclusion for this investigation is presented.

II. Theoretical Background

This chapter provides the necessary information pertaining to the research details that are to follow within the next chapters. A review of nonlinear optics, followed by SBS and SBS threshold is presented. Then, the characteristics of SBS as a phase conjugator are explained and finally, a quick overview of optical fibers will be discussed.

2.1 *Nonlinear Optics*

Light propagating through a medium or through a vacuum may be described by a transverse wave, where the electric and magnetic components are solutions to Maxwell's equations¹¹

$$\nabla \times \mathbf{E} = -(\partial/\partial t)\mathbf{B} \quad (2.1)$$

$$\nabla \times \mathbf{H} = \mathbf{J} + (\partial/\partial t)\mathbf{D} \quad (2.2)$$

$$\nabla \cdot \mathbf{D} = \rho \quad (2.3)$$

$$\nabla \cdot \mathbf{B} = 0 \quad (2.4)$$

where,

\mathbf{E} = electric field

\mathbf{B} = magnetic induction

\mathbf{H} = magnetic field

\mathbf{J} = current density

\mathbf{D} = electric displacement

ρ = charge density

The electric displacement is defined by¹¹

$$\mathbf{D} = \epsilon\mathbf{E} = \epsilon_0\mathbf{E} + \mathbf{P} \quad (2.5)$$

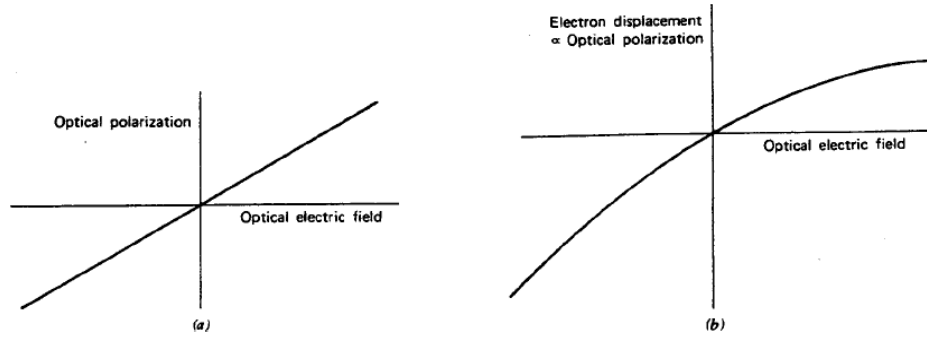


Figure 2.1: Contrast between (a) a linear function, and (b) a nonlinear function¹¹

where,

ε = permittivity

ε_0 = permittivity of free space

\mathbf{P} = polarization

A linear dielectric medium is distinguished by the following equation

$$\mathbf{P} = \varepsilon_0 \chi \mathbf{E} \quad (2.6)$$

where,

χ = electric susceptibility of the medium

\mathbf{E} = electric field

The polarization density is a product of the individual dipole moment induced by \mathbf{E} and the number density of dipole moments. A nonlinear dielectric medium is characterized by a nonlinear relation between the polarization and the electric field.¹²

Figure 2.1 shows a contrast between a linear and a nonlinear function.

As E increases, the electric field deviates slightly from linearity. It is possible to express the function as a Taylor's series expansion at $E = 0$ of the form¹²

$$\mathbf{P} = \varepsilon_o \chi(\mathbf{E}) \mathbf{E} \quad (2.7)$$

$$\cong \varepsilon_o [\chi^{(1)} + \chi^{(2)} \mathbf{E} + \chi^{(3)} \mathbf{E} + \dots] \mathbf{E} \quad (2.8)$$

The first term in this equation is linear and it dominates for small E . The second term represents the second-order nonlinearity, and the third term represents the third-order nonlinearity, and so on. Equation 2.8 states the basic description for a nonlinear optical medium. The induced polarization may be written into a linear and nonlinear parts such that

$$P = \varepsilon_o \chi E + P^{NL} \quad (2.9)$$

where \mathbf{P}^{NL} is the nonlinear component of the polarization density. Inserting this into equation 2.2 with $\varepsilon = \varepsilon_o(1 + \chi)$ and using $J = 0$ for a dielectric material with no free charge or current yields

$$\nabla \times \mathbf{H} = \varepsilon(\partial/\partial t) \mathbf{E} + (\partial/\partial t) \mathbf{P}^{NL} \quad (2.10)$$

Taking the curl of $\nabla \times \mathbf{E}$ from equation 2.1 and using the definition for magnetic induction $\mathbf{B} = \mu \mathbf{H}$, gives

$$\nabla \times \nabla \times \mathbf{E} = -(\partial/\partial t) \nabla \times \mathbf{B} \quad (2.11)$$

$$= -\mu(\partial/\partial t) \nabla \times \mathbf{H} \quad (2.12)$$

$$= -\mu(\partial/\partial t) [\varepsilon(\partial/\partial t) E + (\partial/\partial t) \mathbf{P}^{NL}] \quad (2.13)$$

Since

$$\nabla \times \nabla \times \mathbf{E} = \nabla(\nabla \cdot \mathbf{E}) - \nabla^2 \mathbf{E} \quad (2.14)$$

by using $\nabla \cdot \mathbf{E} = 0$ for a charge free medium we obtain

$$\nabla^2 \mathbf{E} = \mu\epsilon(\partial^2/\partial t^2)\mathbf{E} + \mu(\partial^2/\partial t^2)\mathbf{P}^{NL} \quad (2.15)$$

which is the wave equation in nonlinear optical media. This equation can be seen as the inhomogeneous wave equation where the nonlinear polarization drives the electric field.¹¹

2.2 Stimulated Brillouin Scattering Phenomenon

Stimulated Brillouin Scattering (SBS) is a nonlinear process caused by the third-order contribution to the nonlinearity $\chi^{(3)}$ of a medium. SBS is induced in a medium due to the density variations of the material system.¹² First observed in 1964, this phenomenon manifests itself through the generation of a backward-propagating Stokes wave. This Stokes wave carries most of the input energy once the Brillouin threshold is reached. The frequency is downshifted from that of the pump by an amount established by the nonlinear medium. SBS is normally harmful for optical communications systems but it can also serve for making fiber-based Brillouin lasers and amplifiers.¹³

The best way to fully understand the properties of SBS is to look at the following schematic example in figure 2.3. The pump frequency ω_p , propagates through the medium and encounters an acoustic wave at frequency Ω_B traveling in the same direction. Through the tendency of materials to become compressed in the presence of an electric field or electrostriction¹³.

This generated acoustic wave then modifies the refractive index of the medium. As seen in this example, the sound waves are moving in the same direction as the input beam. Therefore the scattered light ω_s , is downshifted from the original input beam due to the Doppler shift. Conservation of energy and momentum requires that

$$\omega_p = \omega_s + \Omega_B \quad (2.16)$$

$$k_p = k_s + k_B \quad (2.17)$$

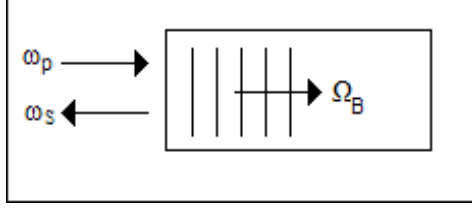


Figure 2.2: Schematic representation of the stimulated Brillouin scattering process.

where the k_p , k_s , and k_B are the wave vectors of the pump, Stokes and acoustic wave respectively. From this it can be determined that the Stokes frequency is given by

$$\omega_s = \omega_p - \Omega_B \quad (2.18)$$

The Brillouin frequency is related to the acoustic wave by the phonon dispersion relation

$$\Omega_B = |k_B| v_a \quad (2.19)$$

where v_a , is the velocity of sound. Since the acoustic frequency is much smaller than the Stokes frequency it can be neglected, therefore we can make the following approximation

$$|k_p| \approx |k_s| \quad (2.20)$$

Then by equation 2.2 and using the relation between wave vectors and frequencies $|k_i| = n\omega_i/c$, yields the Brillouin shift given by¹³

$$\Omega_B = \frac{2nv_a\omega_p}{c} \quad (2.21)$$

The growth of the Stokes beam produced by SBS is characterized by the Brillouin-gain spectrum which peaks at $\Omega = \Omega_B$. Assuming exponential decay of the acoustic waves in the fiber of the form $\exp[-\Gamma_B t]$, SBS has a Lorentzian gain profile and the gain may be calculated by¹³

$$g_B(\Omega) = g_p \frac{(\Gamma_B/2)^2}{(\Omega - \Omega_B)^2 + (\Gamma_B/2)^2} \quad (2.22)$$

where g_p is the peak value of the Brillouin-gain coefficient given by

$$g_p = g_B(\Omega) = \frac{2\pi^2 n^7 p_{12}^2}{c \lambda_p^2 \rho_0 v_a \Gamma_B} \quad (2.23)$$

where n is the modal index at the pump wavelength λ_p , p_{12} is the longitudinal elasto-optic coefficient, and ρ_0 is the material density.

2.3 *SBS Threshold*

Once the Stokes beam is generated in the SBS medium, assuming no pump depletion, the Stokes power increases exponentially. The power being transferred from the pump is redirected to the Stokes beam. To find the SBS threshold, we consider the nonlinear interaction between the pump and the Stokes waves. To obtain the interaction for the CW case, certain assumptions are considered

First, since the Brillouin shift is relatively small, it is assumed that

$$\omega_s \approx \omega_p \quad (2.24)$$

Because of this assumption, it is also expected that the fiber losses are roughly the same for both pump and Stokes wave such that

$$\alpha_s \approx \alpha_p \equiv \alpha \quad (2.25)$$

where

α_s = fiber losses at the Stokes frequency

α_p = fiber losses at the pump frequency

Accordingly for the CW case, the interaction may be expressed as¹³

$$\frac{dI_p}{dz} = -g_B I_p I_s - \alpha I_p \quad (2.26)$$

$$\frac{dI_s}{dz} = -g_B I_p I_s + \alpha I_s \quad (2.27)$$

where

I_s = Stokes intensity

I_p = pump intensity

These equations are derived from the same Maxwell's equations shown in 2.1-2.4. It follows from the assumption made in equation 2.25 that for no fiber losses $\alpha = 0$

$$\frac{d}{dz}(I_p - I_s) = 0 \quad (2.28)$$

which shows that for no fiber losses, the intensity term $(I_p - I_s)$ remains constant throughout the fiber.

For the purpose of estimating the SBS threshold, pump depletion can be disregarded. Using the pump intensity to be

$$I_p(z) = I_p(0)e^{-\alpha z} \quad (2.29)$$

where z is the direction of propagation, substituting this into equation 2.26 and rearranging the terms gives

$$I_s(0) = I_s(L) \exp\left(\frac{g_B P_0 L_{eff}}{A_{eff}} - \alpha L\right) \quad (2.30)$$

where

$P_0 = I_p(0)A_{eff}$, input pump power

$A_{eff} = \pi w^2$, effective core area for a Gaussian beam, where w is the mode field radius

$$L_{eff} = \frac{[1 - \exp(-\alpha L)]}{\alpha}, \text{ effective interaction length}$$

This shows how the intensity of the Stokes beam grows exponentially in the backward direction due to SBS in the medium. Then, the Brillouin threshold can be approximated by¹³

$$\frac{g_B P_{th} L_{eff}}{A_{eff}} \approx 21 \quad (2.31)$$

where

g_B = peak value of the Brillouin gain

An example of this approximation using typical values used in optical communication systems for $\lambda = 1.55 \mu m$ has the values of

$$A_{eff} = 50 \mu m^2$$

$$L_{eff} = 20 \text{ km}$$

$$g_B = 5 \times 10^{-11} \text{ m/W}$$

By equation 2.15 it can be seen that the SBS threshold is close to $\approx 1 \text{ mW}$. Because of the low thresholds, SBS is the dominant nonlinear process in fibers for narrow frequency operation, compared to SRS which has a relative higher threshold.¹³

2.4 Optical Phase Conjugation

Optical phase conjugation (OPC) refers to optical devices that can generate a time-reversed replica of an incident electromagnetic wave.¹⁴ Figure 2.3 shows a schematic representation of this process. First, a planar wave front is shown traveling in the z direction. As the wavefront propagates through the distorting medium, a phase delay is created in the wavefront which is now no longer in planar.

In the first case, the wavefront is inverted horizontally when the conventional mirror is used for reflecting the beam back in the direction of the incident wavefront. This makes the wavefront travel through the distorting medium for a second time, thus increasing the wavefront error by the same amount as the first pass. For the second case, the wavefront seems to be time reversed by the PCM. As the wavefront propa-

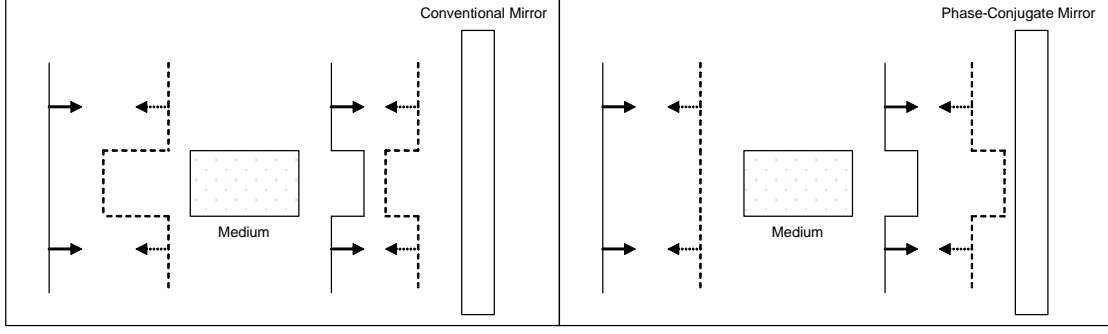


Figure 2.3: Comparison between a mirror and a phase-conjugation mirror.

gates back through the same distorting medium, the wavefront error is corrected. This can also be explained analytically through the following example. Consider the propagation of a wave in the z direction. Let the electric field be expressed as¹⁴

$$E = A(r)e^{i(\omega t - kz - \phi(r))} \quad (2.32)$$

where

A = amplitude

ϕ = phase

z = direction

ω = angular frequency

t = time

k = wavevector magnitude

If we defined a complex quantity as

$$A_1(r) = A(r)e^{i\phi(r)} \quad (2.33)$$

then equation 2.32 can be written

$$E = A_1(r)e^{i(\omega t - kz)} \quad (2.34)$$

The phase conjugate of this beam is computed by taking the conjugate of the spatial part only

$$E_c = A_1^*(r)e^{i(\omega t + kz)} \quad (2.35)$$

which states that the phase conjugate of the input wave propagates in the -z direction with complex magnitude A_1^* . Then, as the beam propagates backward in the -z direction, it follows the same path previously traveled by the forward incident beam. The amplitude and phase of the backward moving beam are equal to that of the incident beam.

2.5 *Optical Fibers*

In order to obtain a Stokes wave, an SBS medium is needed. For this research, the beam cleanup and phase conjugation properties of multimode optical fiber were studied.

To begin the development of this topic, consider the relationship by which light is refracted as it propagates from one isotropic media to another. This is known as Snell's law which states that¹⁵

$$n_1 \sin[\theta_1] = n_2 \sin[\theta_2] \quad (2.36)$$

where

n_1 = index of refraction of incident beam

n_2 = index of refraction of refracted beam

θ_1 = angle of incidence

θ_2 = angle of refraction

For light propagating from a medium with lower index of refraction to a higher one, the incident light bends towards the normal. This process is depicted in figure

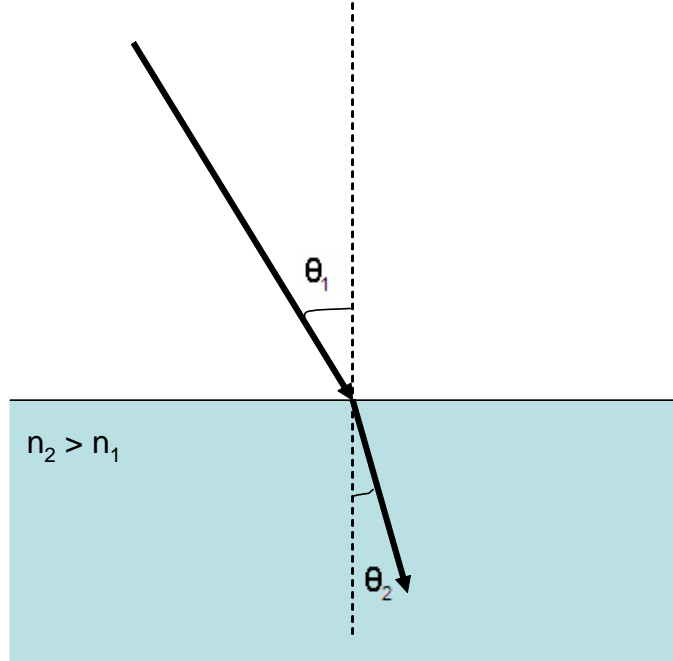


Figure 2.4: Snell's law for a ray going from n_1 to a surface of index n_2 .

2.4. In contrast, when light propagates from a higher to a lower index of refraction, light bend away from the normal.

An interesting phenomenon occurs when light travels from a high index to a low index of refraction. Light will be completely reflected for incident angles larger than the critical angle θ_c . The critical angle can be determined from Snell's equation by setting the angle of refraction at 90° such that

$$n_1 \sin[\theta_1] = n_2 \sin[90^\circ] \quad (2.37)$$

Solving for θ_1

$$\theta_1 = \theta_c = \sin^{-1} \left[\frac{n_2}{n_1} \right] \quad (2.38)$$

where θ_c is the critical angle. For angles of incidence equal or larger than θ_c , all incident light will be totally internal reflected back into the same medium as the incident light.

Optical fibers, shown in figure 2.5, are cylindrical dielectric waveguides. They are composed of a central core in which the light travels through the fiber. This core is surrounded by a cladding of a slightly lower refractive index than the core region. Both of the regions are protected by a buffer or jacket to prevent damage to the fiber. This process of guiding light is driven by the process of total internal reflection.

Figure 2.6 shows the process in detail. For a ray incident from the air into the optical fiber, light will be guided if the transmitted beam propagating in the core makes an angle smaller than that of the critical angle at the boundary between the core and the cladding. The term θ_a expressed in these equation is known as the acceptance angle of the fiber. This angle determines the cone of the external rays that are disseminated in the fiber. For total internal reflection to occur¹⁵

$$\theta_1 > \theta_c \quad (2.39)$$

The angle θ'_1 is the angle that the incident light in the fiber makes with respect to the normal at the entrance. Since θ_1 and θ'_1 are complementary angles, they can be related as

$$\theta_1 < 90^\circ - \theta_c \quad (2.40)$$

Applying Snell's law to the air/core boundary

$$n_0 \cdot \sin[\theta_a] = n_1 \sin[\theta'_1] \quad (2.41)$$

by equation 2.40 this becomes

$$n_0 \cdot \sin[\theta_a] < n_1 \sin[90^\circ - \theta_c] \quad (2.42)$$

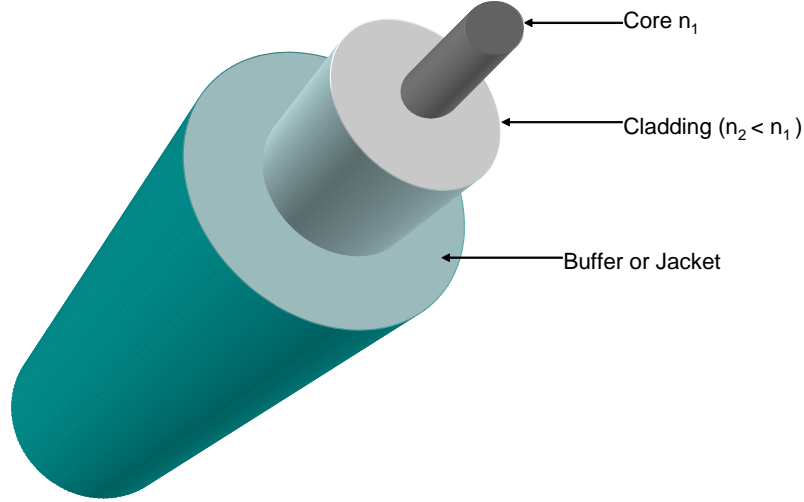


Figure 2.5: Representation of an optical fiber exhibiting the core, cladding, and buffer/jacket regions..

Using trigonometric identities in the previous equation yields

$$n_0 \cdot \sin[\theta_a] < n_1 \cos[\theta_c] \quad (2.43)$$

finally

$$n_0 \cdot \sin[\theta_a] < n_1 [1 - \sin^2[\theta_c]]^{1/2} \quad (2.44)$$

By substituting in equation 2.38 and solving for θ_a gives

$$\theta_a = \sin^{-1}[NA] \quad (2.45)$$

where

$$NA = \sqrt{(n_1^2 - n_2^2)} \quad (2.46)$$

is the numeral aperture of the fiber which describes its light-gathering capacity. Light in optical fibers propagates as modes. Each of these modes travels along the waveguide with a distinct propagation constant and group velocity.¹² Generally, there are two types of optical fibers - single mode and multimode. A single mode

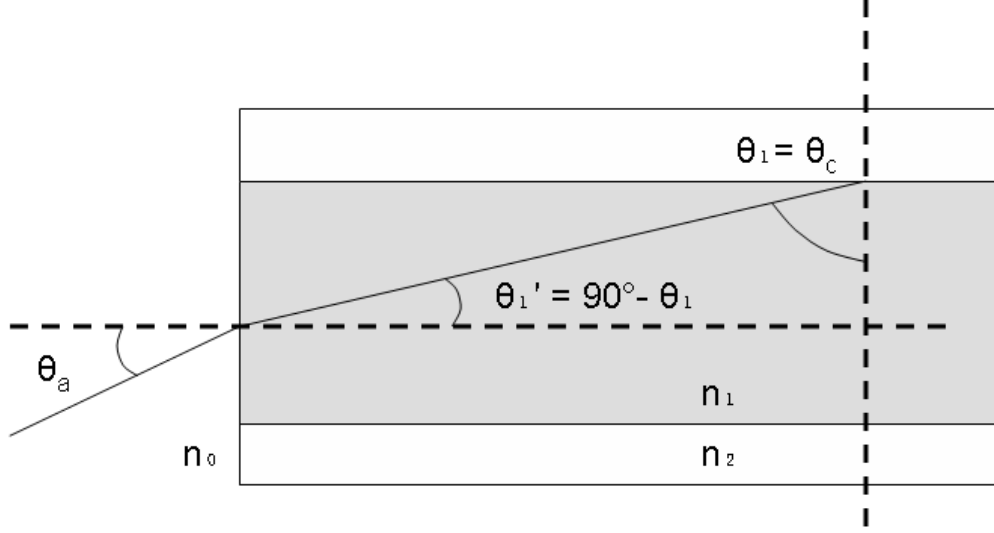


Figure 2.6: Propagation of light inside an optical fiber.

fiber usually has a smaller core and only allows for one mode of light to propagate at a time. Multimode fiber usually has a larger core than that of a single mode fiber but it allows for numerous modes to propagate simultaneously through the waveguide.

The lowest order mode that propagates in optical fibers is known as the fundamental mode LP_{01} . The spatial distribution of this mode is represented in figure 2.7. By looking at the same profile in 3D, figure 2.8, it can be seen that it closely resembles that of a Gaussian beam. These two computationally developed beam profiles resemble those obtained in the next chapter in an experimental setting using multimode fibers as a SBS medium.

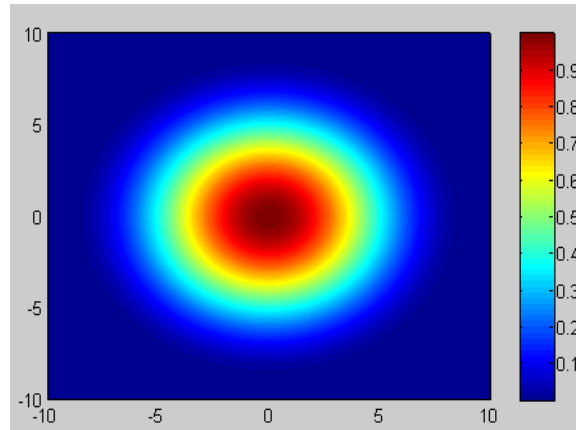


Figure 2.7: Computer generated 2D plot exhibiting the fundamental fiber mode LP_{01} .

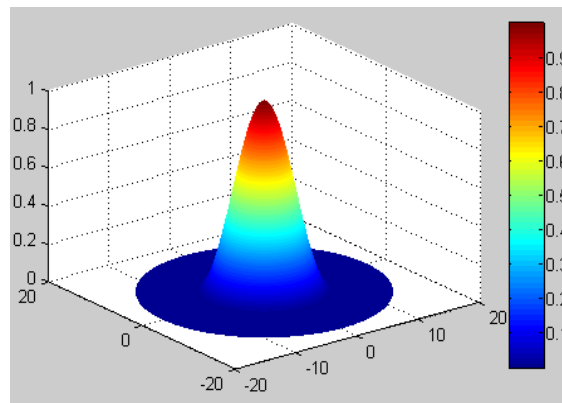


Figure 2.8: Spatial distribution in 3D of the LP_{01} mode. Notice that the intensity profile is similar to that of a Gaussian beam.

III. SBS Beam Cleanup

This chapter describes the experimental setup and results for the study of SBS beam cleanup properties by means of a multimode optical fiber. The chapter begins with a brief background description on the beam cleanup results obtained from past experiments. Section 3.2 describes the methodology used to demonstrate the feasibility of long multimode fiber as a beam cleanup device and the results for this experiment.

3.1 *Background*

The beam cleanup properties of SBS play an important role into this research because this process is believed to have a significant impact in the phasing properties of SBS. By using a long multimode fiber, the beam cleanup process was first observed by Bruesselbach, and demonstrated by Rogers, Grime, and others.^{8,10,16} It was shown that the SBS phenomenon creates a Stokes beam with an intensity distribution which corresponds to the fundamental fiber mode LP_{01} . This means that a distorted beam may be cleaned by means of coupling the beam into a long multimode fiber. The beam cleanup property of long multimode fibers is believed to occur as a result of the higher gain exhibited by the LP_{01} mode over higher order modes of the Stokes beam in the presence of a multimode pump.⁸

3.2 *Experiment and Results*

In order to observe SBS cleanup in a multimode fiber, the following experimental process was developed. The source for this research consisted of a Non Planar Ring Oscillator (NPRO) producing around 700mW at $1.06\mu m$. A two pass Nd:YAG rod amplifier developed by Cutting Edge Optics amplified the beam to a maximum power output of $\sim 1.4W$.

As shown in Figure 3.1, the NPRO output is transmitted through a telescope to reduce the amount of divergence throughout our system and focus the beam into the amplifier. The beam is then reflected by 90° using an HR mirror and aligned to pass through a halfwave plate. After this, a polarizing beam splitter (PBS) is added.

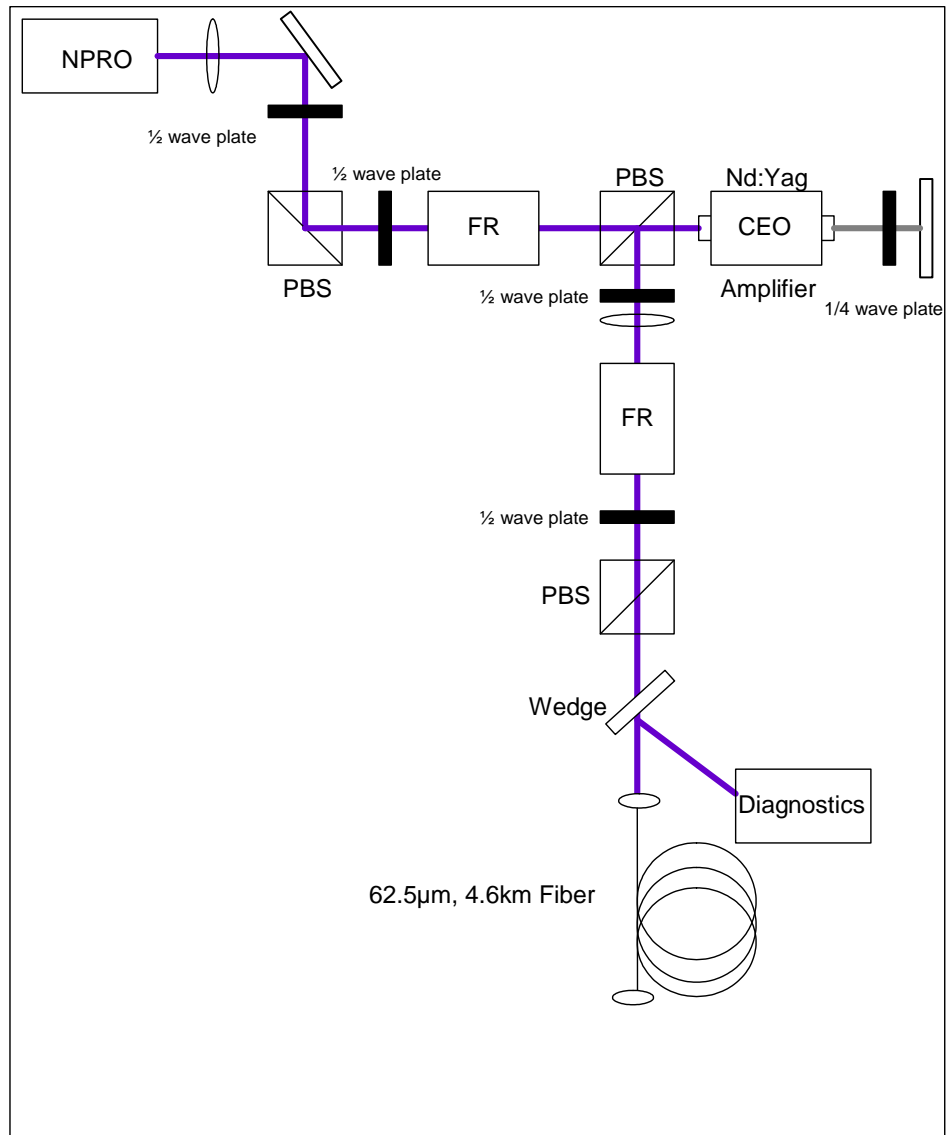


Figure 3.1: Experimental setup used to demonstrate the SBS beam cleanup properties of a long multimode fiber.

The beam then passes through a Faraday rotator, another halfwave plate and a PBS. This setup was used to prevent feedback from reaching into the NPRO. This beam goes through the amplifier twice as it goes through a quarter wave plate, reflecting from the dielectric mirror and propagating once again through the Nd:YAG amplifier. Finally, the output of this is then reflected off from the PBS.

Once this amplifier was proven to work and that the output power was sufficient to reach SBS threshold, another Faraday rotator followed by a halfwave plate and PBS were used to prevent feedback from the fiber from going into the amplifier. In order to observe the Stokes beam as it propagates out of the fiber, a beam pickoff needed to be used. For this experiment, a wedge with one side AR coated was used to measure the power of the Stokes beam, the SBS frequency shift, and to observe the spatial intensity profile with a CCD Camera. The fiber was a 4.6 km long $62.5\ \mu\text{m}$ core multimode fiber.

When the setup was completed, the maximum pump power that was coupled into the fiber was about 800mW. The transmitted power through the fiber as a function of the input power coupled into the fiber is shown in Figure 3.2. As the power coupled into the fiber is increased, it was discovered that the transmitted power increased at a consistent rate for power readings below $\sim 500\text{mW}$. For input values above threshold, the transmitted power increase rate is reduced. When the power inside the fiber reaches SBS threshold, a greater amount of the input power goes into the backward moving Stokes beam. Figure 3.3 presents how the Stokes power increases once threshold has been reached. The value forecasted for the SBS threshold from the equations shown in chapter 2 placed the threshold to be around 480mW for this experiment. This can be seen in figure 3.3 as a sudden increase in contrast with the input vs transmitted power plot, where the growth of the transmitted power increases at a fairly steady rate. Note that the first sudden increase in figure 3.3 for input power of 100mW is due solely to a change in the range of the power meter. The error bars are due to pulsing when the Stokes beam reached the amplifier.

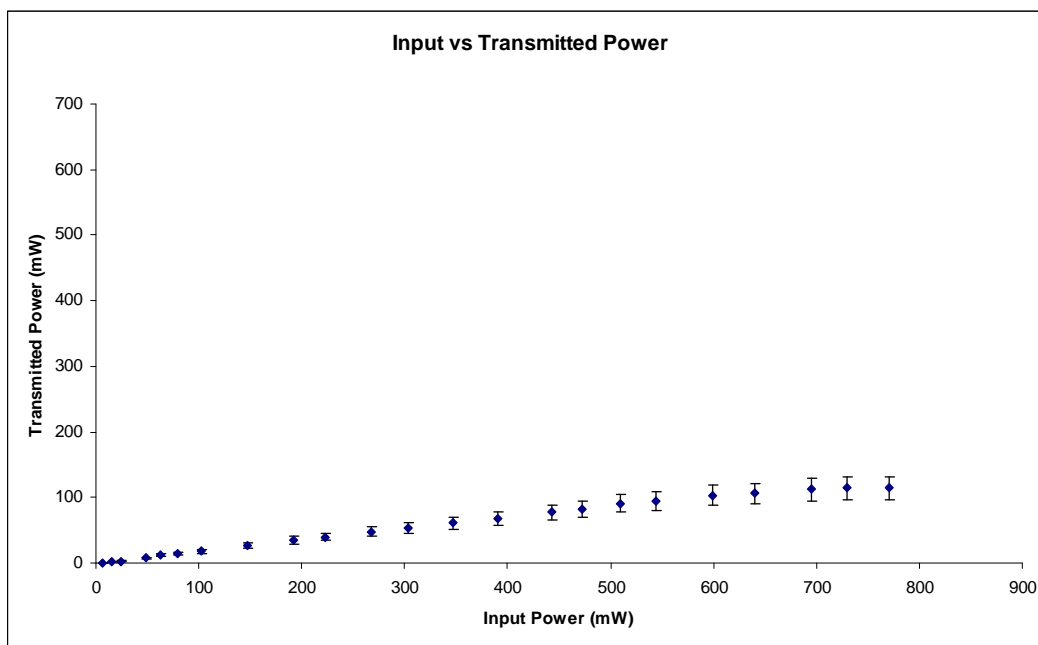


Figure 3.2: Input power as a function of the input power.

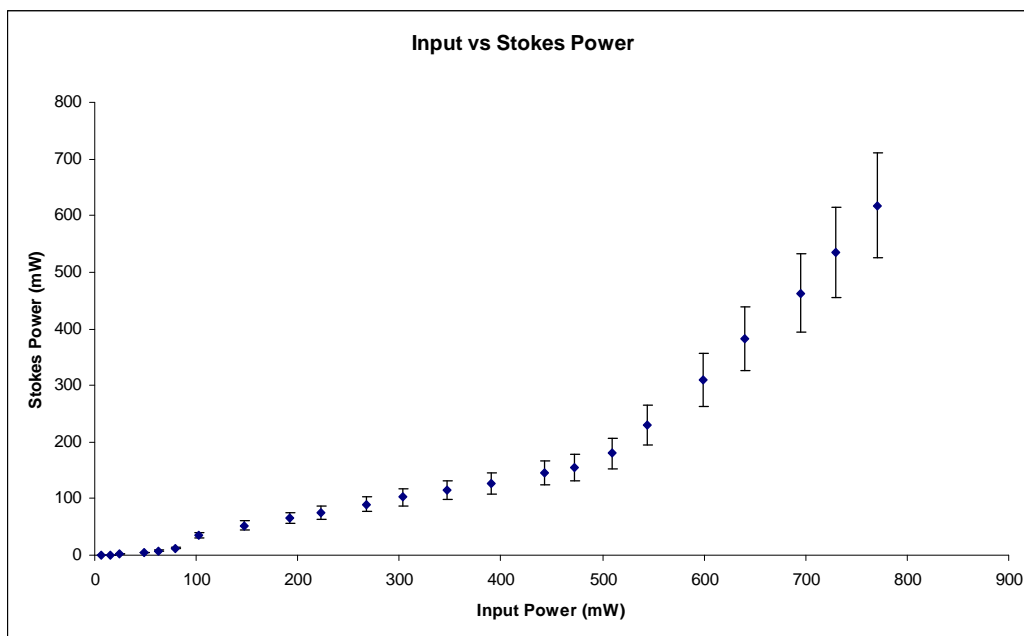


Figure 3.3: Stokes power as a function of the input power.

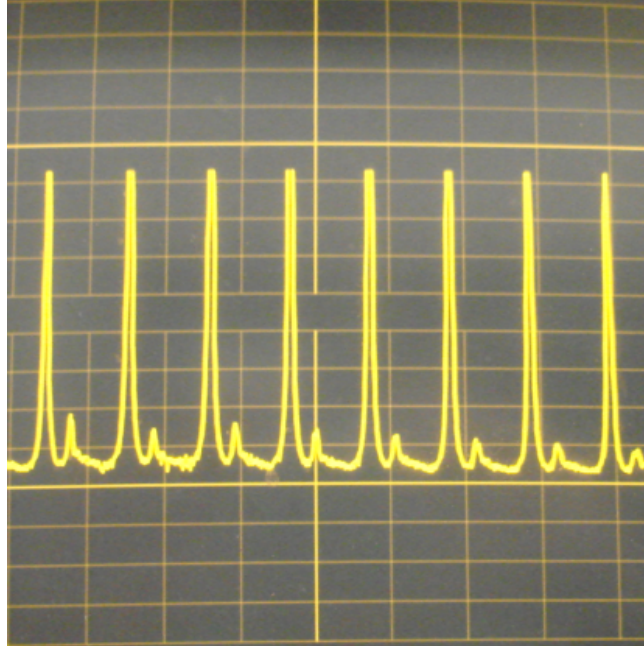


Figure 3.4: Oscilloscope view showing the data obtained with the Fabry-Perot spectrum analyzer.

Besides measuring the Stokes power, the beam pickoff was also utilized to quantify the SBS frequency shift. To do this, a Fabry-Perot spectrum analyzer scanner was used to observe and to record the frequency shift, which is usually in the order of GHz. The Fabry-Perot data is shown in Figure 3.4 for pump power above SBS threshold. The SBS frequency shift can be measured by characterizing the output using the known free spectral range (FSR) of the spectrum analyzer. The Fabry-Perot used for this research had a FSR of 8 GHz.

As demonstrated in chapter 2, we can estimate what the SBS frequency shift would be for this experiment. Using equation 2.31 for a laser at $1.06\mu m$, with silica fiber of refractive index $n = 1.45$ and acoustic velocity of 5.96 km/s results in a SBS frequency shift of $\sim 16.2\text{ GHz}$. Since this shift is greater than the FSR of the spectrum analyzer, we need to correctly determine which Stokes peak frequency corresponds to which pump peak. The schematic representation of how this procedure is performed is shown in Figure 3.5. Since the FSR of the spectrum analyzer is 8GHz, it can be

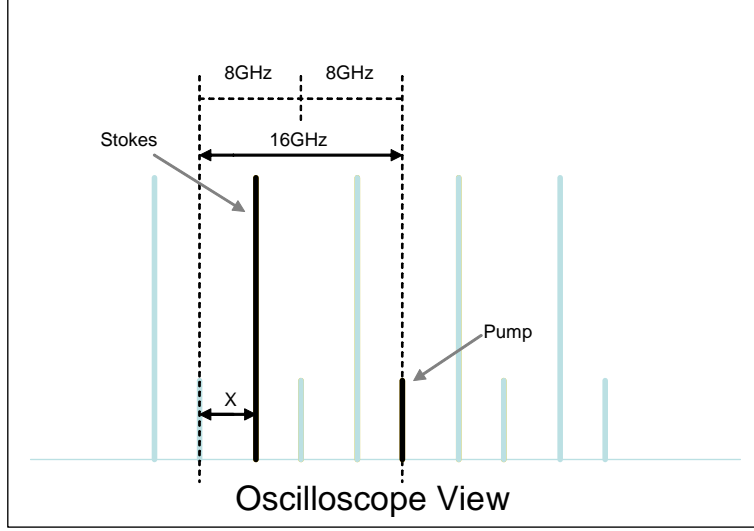


Figure 3.5: Representation of the procedure used to measure the SBS frequency shift.

seen here that the Stokes related to the pump is shifted by 14.1 GHz, which is the SBS frequency shift of our system.

The last step of this experiment consisted of inserting a beam aberrator into our system to determine if the long multimode fiber generates a backward propagating Stokes beam within the LP_{01} mode regardless of the pump beam being coupled into the fiber. The left side in figure 3.6 shows the beam profile of the pump beam before being coupled into the fiber and the right side shows the Stokes profile obtained from the $62.4\mu m$ core multimode fiber after a single pass through the aberrator. By comparing the two beam profiles, it can clearly be seen that a Gaussian-like beam is generated in the fiber. These results prove that when SBS is produced inside of a long multimode fiber, a Gaussian-like beam is retro-reflected by the fiber.

3.3 Conclusion

The results presented in this chapter are in agreement with previous experiments carried out by various researchers through the course of several years.^{8,10,16} When SBS takes place inside of a long multimode fiber the resulting Stokes beam will propagate in the fundamental mode. It can be stated that a phase conjugate reflection of

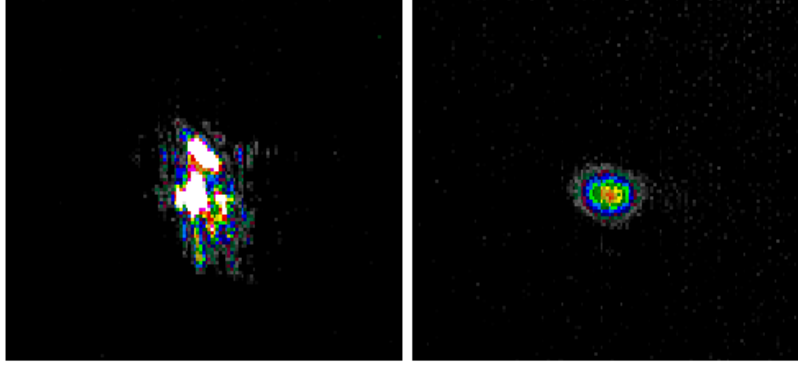


Figure 3.6: Beam profile of aberrated beam (left) and the Stokes beam generated before double-passing the aberrator (right).

the input beam was not produced by the long multimode fiber, that is, the SBS medium. Instead, it was observed that SBS in the fiber produced a Stokes beam with Gaussian-like profile independent of the spatial distribution of the pump beam. Thus, when the aberrated pump beam is used to excite SBS in a long multi-mode fiber, the SBS process has the effect of cleaning up the beam aberrations to produce a clean Gaussian-like Stokes beam.

IV. Beam Phase Conjugation of Two Passive Channels

This chapter explores the properties of SBS, namely for the purpose of phase conjugating a beam in a multimode fiber. A brief review of past results and theory related to this experiment is presented. Then, the experimental setup used to investigate this property is explained followed by the results and how these compare to past results.

4.1 Background

Over the last three decades, optical phase conjugation (OPC) has been a major research topic in the nonlinear optics field¹⁷. It provides a method by which beam quality can be improved and by which power combining from multiple laser can be combined.^{17,18}

One method for beam combination suggests the use of a single master oscillator in which the source is split into multiple beams that travel through different channels. Each channel is individually amplified and then combined to obtain a single beam with an output equal to the combination of all the channels. This procedure proves to be inadequate due to a phase delay created between the path length differences between these channels.⁶ When focusing the total output beam it is desirable to have each individual beam match in phase in order to achieve maximum intensity in the far field.

The nonlinear optics solution seeks to exploit the properties of SBS phase conjugation in a medium to eliminate the wavefront error produced by the differences in path length. This phenomenon has a unique feature by which any aberrations imposed on the forward beam as it passes through a certain disturbing medium can be removed as the beam is retro-reflected from the PCM and retraces its path through the same medium.

Several experiments have been developed regarding the characterization of this SBS property. Basov *et al* was the first person to successfully correct the phase delay between channels by separating a single laser source into two beams.¹⁹ These were then later recombined into an SBS cell. The SBS cell acted as a PCM and the phase

conjugate output beam traveled backwards through the same path, thus correcting the wavefront error.

Three important results were stated from his research. One of them stresses the importance of combining all the channels into the same SBS medium. This is due to the random SBS generation from thermal noise in a medium. Inducing SBS inside two separate mediums would produce a random relative phase between them such that no phase conjugation would be observed. The second statement relates the SBS frequency shift, Δ_B , and the allowed path length difference, Δ_L , to the relative phase error, δ , after the second pass through the aberrator as

$$\delta = \Delta_B \Delta_L \quad (4.1)$$

The relative phase error requires accurate control of the optical path difference between the channels to obtain piston correction.

In another subsequent research developed by Moyer *et al*, SBS was investigated with the purpose of combining multiple laser beams⁵. The source in his experiment consisted of a frequency tripled Q-switched Nd:YAG laser. As shown in figure 4.1, the research approach to studying SBS as a PCM resided in using what he called clipper mirrors to spatially split the source into two semicircular beams. Each beam was then fixed to travel through its own individual channel. Two mirrors were positioned in what is called a trombone arm, capable of moving in one dimension such that one of the channels path length could be varied in such a way that the phase delay between paths could be increased or decreased.

The principal diagnostic tool used to detect for piston error conjugation was the lateral shearing interferometer (LSI), shown in the center of figure 4.1. The LSI in this configuration consisted of two uncoated wedges arranged nearly parallel to each other. Figure 4.2 shows a schematic representation of the setup using the LSI for the two semicircular beams. The two inner reflections from the LSI are tiled next to each other such that the interference pattern of these beams can be observed. The

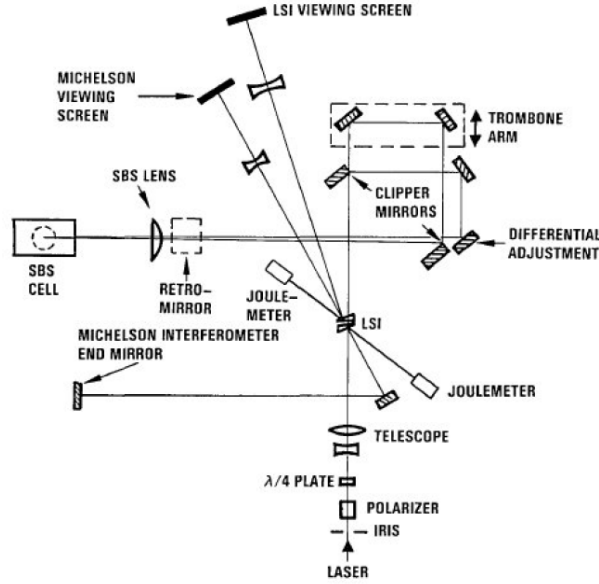


Figure 4.1: Optical layout for overlap-coupling experiment developed by Moyer *et al.*⁵

interference in left side is due to the first beam reflecting of the two surfaces in the LSI. The right side of the interference is due to the two reflections of beam two from the LSI. The middle region represents the mutual interference pattern between beams 1 and 2. As the trombone arm is displaced, the fringes in this middle region move as a result of changes in path length between the two channels. As the phase delay is varied, the right and left side of the interference pattern remain the same since a beam, no matter which path it takes, interfering with itself will always give a steady interference.

In this investigation, as well as in several others, the SBS phase conjugating mirrors used consisted of using cells filled with liquids or gases under high pressure¹⁷. These expressed that when using an SBS cell, the system was very sensitive to misalignment and requires the beams to be overlapped in a common focal volume within the medium. In contrast, when optical fiber is used as the SBS medium, these alignments problems are eliminated because the beams are enclosed inside of the core in a fiber such that the beams are overlapped in a long interaction length. This definite

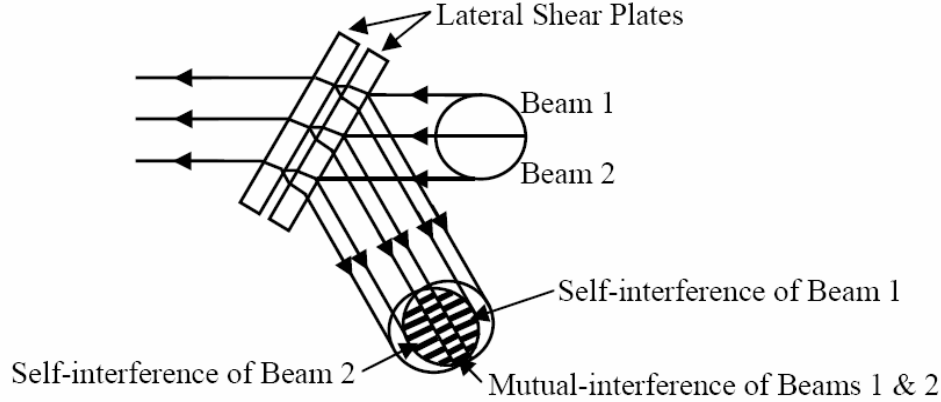


Figure 4.2: Lateral shearing interferometer (LSI) for two semicircles that travel through different channels. The interference produced using the LSI is the diagnostic tool to determine piston error conjugation.

advantage of using optical fibers as SBS phase conjugating mirrors motivated research in this area.

A recent experiment concerning the use of short multimode fiber was developed by Willis.⁶ Figure 4.3 shows the experimental setup for testing short multimode fiber as a possible PCM.

In this experiment, a Nd:YAG Q-switched laser was used as the laser source. The separation mechanism of the beams consisted of four right angle prisms arranged fairly similar to that shown earlier by Moyer *et al.* The first right angle prism is used as a pickoff which spatially separates the beam into two portions. After the beams traveled different paths, they are tiled side by side and coupled into a short ($<10\text{m}$) $600\mu\text{m}$ core multimode fiber. Unfortunately, as the Stokes made its way back, the results from the LSI made using microscope slides were somewhat inconclusive and another test was perform to determine the coherence of the beams as they left the fiber. In short, it was determined that in fact the Stokes beams leaving the fiber were coherent and that phase conjugation was possible for short multimode fiber.

Several problems with this method were underlined by Willis when the Q-switched laser was implemented for this experiment. This pulsed laser lead to pulses of very high peak power which in turn made it difficult to couple the light into the

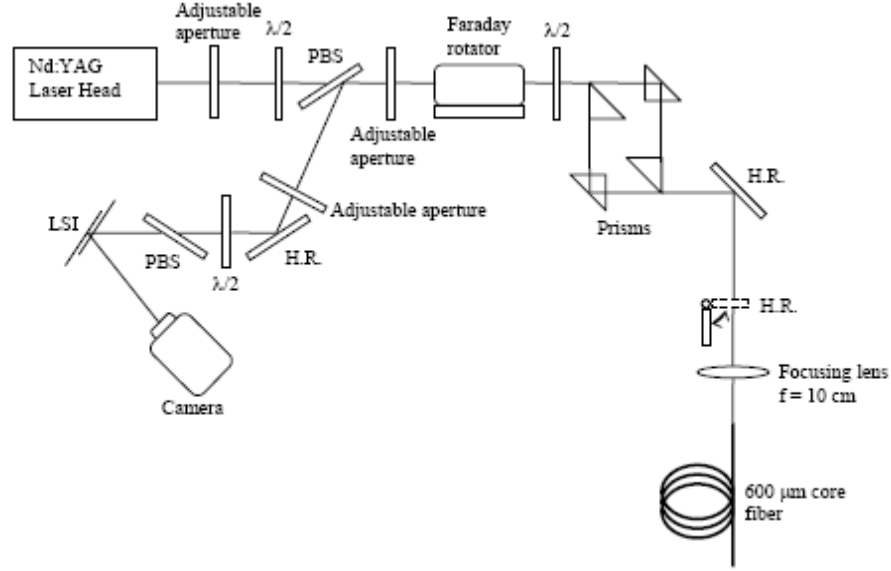


Figure 4.3: Experimental setup of a short multimode fiber as a PCM by Willis *et al.*⁶

fiber without damaging it. Because of this, another experiment concerning multimode fibers as a PCM was developed by Grime¹⁰. In his experiment, a similar two passive channel setup as that previously used by Moyer and Willis was developed using a single-frequency CW laser as the input source. Additionally, the fiber length was increased, in km, in order to reach SBS threshold using a CW source. In the end, it was shown that phasing of two beam paths was achieved even when a spatial conjugate of the beam was not produced due to the length of the fiber, which was shown in chapter 3 as well as by several others researchers to produce a Stokes beam with fundamental fiber mode LP_{01} for long lengths of fibers.¹⁶

The property of SBS in multimode fibers has been demonstrated to change depending on the length of the fiber in use. Short multimode fiber produces a phase conjugate of the pump beam coupled into the fiber. However, there is some debate over whether SBS in long multimode fiber produces a phase conjugate of the pump beam. In chapter 3, it was shown that SBS in long multimode fiber produces a Stokes beam that has a spatial distribution of a Gaussian-like beam, meaning that the LP_{01} fiber mode is excited inside the optical fiber.

The length at which this property changes from one to another is also debated. One expression for the maximum fiber length in which phase conjugation can be observed is²¹

$$L \leq \frac{6r_0^{1/2}c\pi}{\Delta\omega(NA)} \quad (4.2)$$

where

L = maximum length of fiber

r_0 = allowable non-phase-conjugation fraction

NA = numerical aperture

c = speed of light

$\Delta\omega$ = Stokes frequency shift

According to the author, by taking $r_0 = 0.1$ and $NA=0.2$ and using a pump wavelength of 1064nm, the maximum allowable length of the fiber for SBS phase conjugation should be no more than 0.5m. Another estimate developed earlier suggests that the allowable length of the fiber is given by²²

$$L \leq \frac{10Mc}{\Delta\omega(NA)^2} \quad (4.3)$$

where

M = coefficient dependent on the mode distribution of the pump

This M coefficient has an order of magnitude of around 10. This suggests that the maximum fiber length for phase conjugation should be around 10 times greater than that obtained with equation 4.2. This would result in a fiber of no more than $\sim 5m$.

It is important to keep in mind that these values should better be used just as reference. In the research implemented by Willis, it was found that a multimode fiber $\sim 10m$ in length produced the phase conjugate of the pump beam.

In this research, a similar investigations performed. However, in this case, the LSI and the experimental setup is implemented in such a way that the boundary regions between the self interference of beams 1 and 2 together with the mutual beam interference can be prominent allowing for a better distinction of fringes. By doing so, it is shown that the beam cleaning properties of long multimode fibers, prevent the phase conjugate of the pump beam to be excited inside the fiber.

4.2 Experiment and Results

To analyze the phase conjugation properties of a long multimode fiber, the setup shown in Figure 4.4 was constructed. For this part of the experiment, we utilize the same laser source described in the previous chapter. It consisted of an NPRO with a two pass Nd:YAG amplifier which provides a maximum output power of $\sim 1.4\text{W}$. To control the output obtained from the two pass amplifier, a half wave plate and polarizer are placed in the beam. By rotating the wave plate, the amount of transmitted power can be varied. After this, a beam expander is placed in the system. This aids in the process of spatially dividing the beam. Then the LSI is placed where the Stokes reflection is to be analyzed. The beam is then divided into to halves or semicircles of equal power. The right half of the beam travels through a straight channel and the path length is unchanged during the entire duration of this experiment. The left side of the beam however is picked off using a right angle prism and travels through a separate channel. This channel has a movable piezo electric stage that allows for path length variation on the order of a few wavelengths. After both of these halves have gone through their respective channels, the two beams are tiled side by side and coupled in the $62.5\ \mu\text{m}$ core multimode fiber.

Figure 4.5 depicts the beam profile before each side is spatially separated into the two channels. The right half goes through the fixed channel while the left side is diverted to pass through a second channel, which contains the embedded movable stage. Figure 4.6 shows the resulting beam as viewed after each beam traveled its own



Figure 4.5: Beam profile before being separated into two channels.

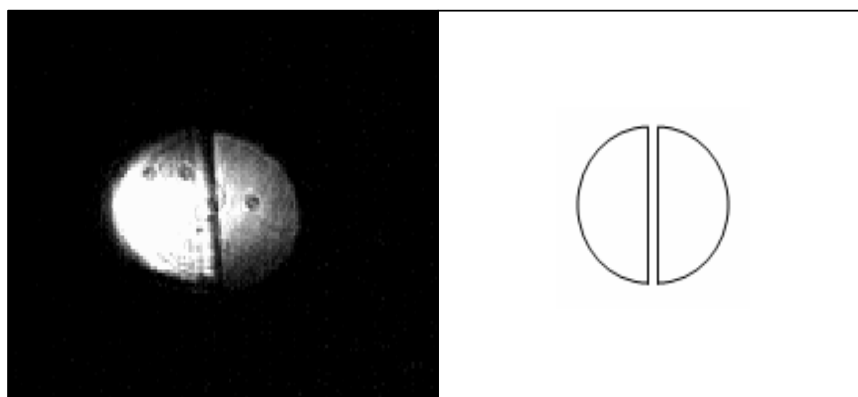


Figure 4.6: Beam profile after beam goes through separate paths and then rejoined.

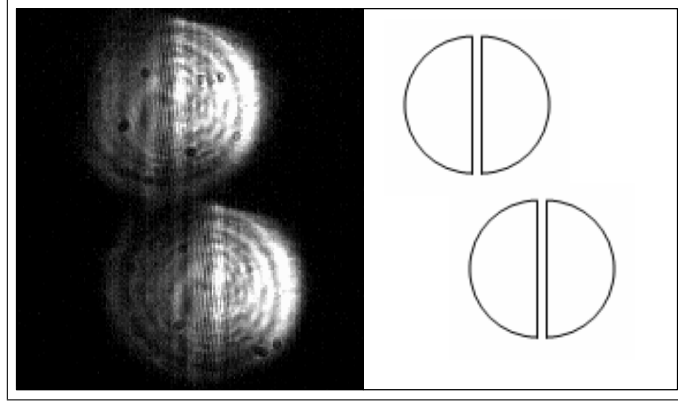


Figure 4.7: Two reflections from LSI.

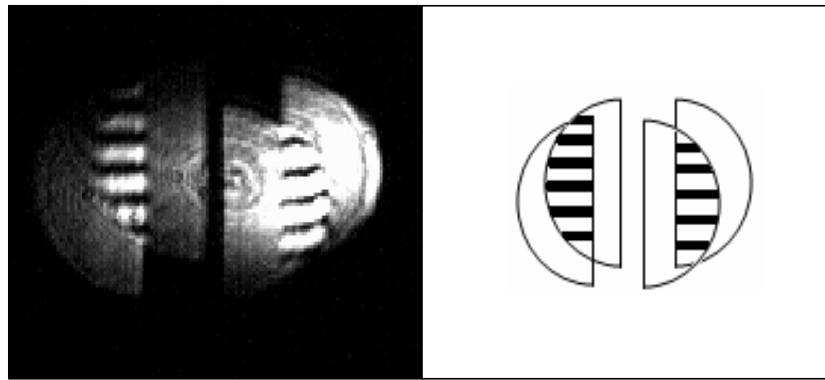


Figure 4.8: Self-interference between the two reflections from the LSI.

superimposed to create the self interference of the beams seen here. The right side shows the self interference of the beam traveling through the first channel while the left side shows the self interference of the beam traveling through the second channel.

Then, the two reflections are brought together to form the interference pattern created by the combination of beams 1 and 2. This is shown in Figure 4.9, where the three regions of interference can be clearly depicted. Since we are using a conventional mirror, the profile shows that there is no continuity throughout the three regions. Because the fringes of the self interference of beams #1 and #2 are not aligned to the mutual interference created by both beams, which is located at the central region of the beam profile, then the beams are shown to be unphased.

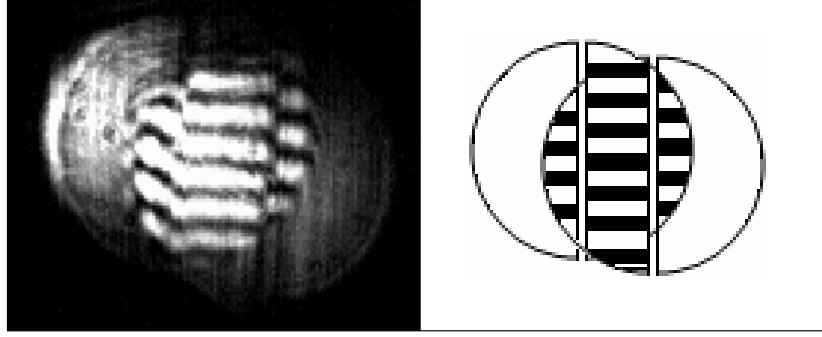


Figure 4.9: Interference showing that the beams are not in phase.

Once the LSI was characterized, the HR mirror was replaced with the multimode optical fiber used in chapter 3 for the SBS beam cleanup properties. Enough power is then coupled into the fiber to reach SBS threshold. Once attained, the Stokes reflection propagating from the optical fiber was analyzed with the Fabry-Perot spectrum analyzer to assure that there was a frequency shift. The resulting Stokes beam is shown in figures 4.10 and 4.11. These two reflections are then examined using the LSI. The result of the beam viewed through the LSI just after exiting the fiber is shown in Figure 4.12. The two reflections from the LSI reveals that the two semicircles of beams have been cleaned and now exhibit a profile of a Gaussian beam. Even when the pump beam exhibited a profile with two beams side by side, SBS in the fiber generated a Stokes beam with no spatial divisions. From the results obtained in chapter 3 and the evident Stokes output, it can be said that when the SBS threshold is reached inside long multimode fiber, beam cleanup occurs and the generation of the LP_{01} mode is obtained. This becomes more evident in the 3D plot depicted in Figure 4.11. When the two beams are combined to observe the interference properties of the Stokes, the attained interference fringes shown across the three regions were in fact continuous throughout the three boundaries. This demonstrates that the backward moving Stokes immediately exiting the fiber is phased. Because the beams are phased as they leave the fiber, no phase conjugation is expected to occur after the second pass through the system.

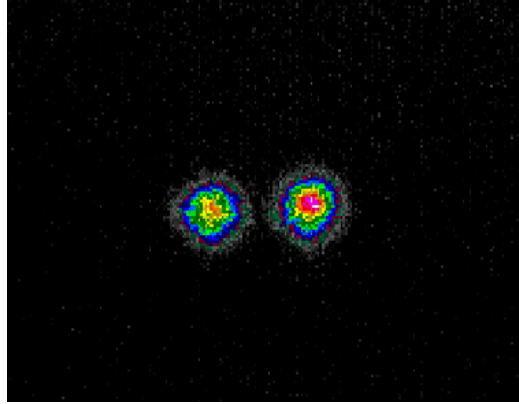


Figure 4.10: Two reflections from the Stokes beam just after exiting the fiber. Here, the two beam reflections appear to be the fundamental mode LP_{01} .

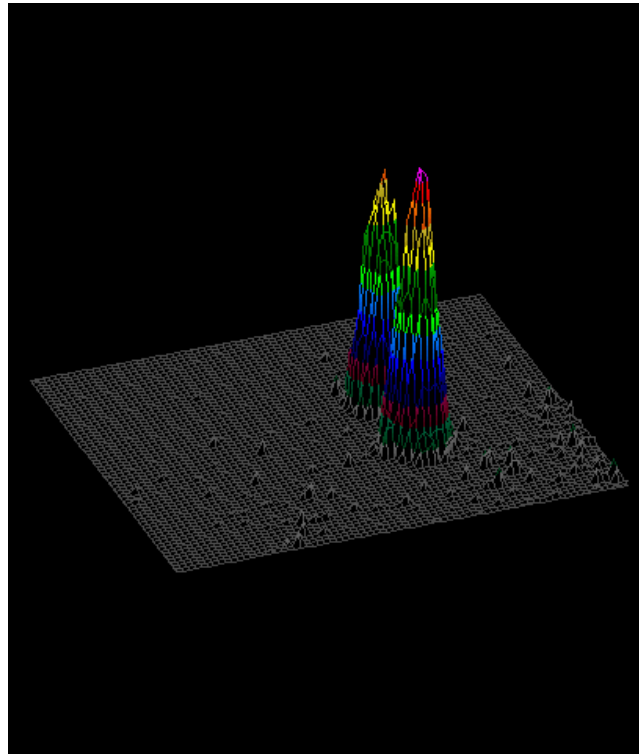


Figure 4.11: 3D profile of the two reflections of the Stokes just after exiting the fiber. The beams are now continuous and the division between the beams has dissappeared due to beam cleanup.

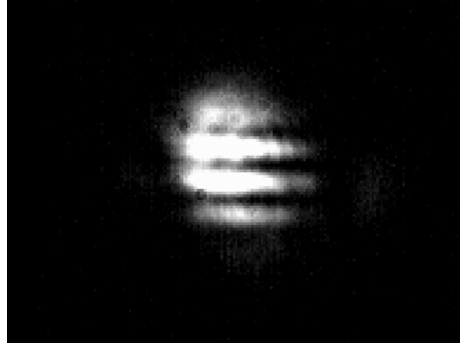


Figure 4.12: Interference pattern showing that the two sides of the beam are phased. The reflections that create this interference come from the two reflections of the Stokes beam immediately after exiting the fiber.

With results expressing that the Stokes beam right after propagating out of fiber is in fact phased, the backward moving beam is then allowed to travel through the two channel system once more, where each side of the beam retraces its own path back to where the beam was originally spatially divided. By using the second LSI embedded in our optical system, we obtain the results shown in Figure 4.13. Because of the movement sensitivity of the system and the need for more precise way of alignment the equipment for this experiment, it was difficult to obtain a more defined beam as that obtained in figure 4.9. Nevertheless, the results show well defined boundaries between each region. The three boundary regions are shown in detail. The left side is self interference of beam #1. The right side shows self-interference of beam #2. The mutual interference of the beams is depicted in the central region. The fringes are not continuous across the regions as it was the case for figure 4.12. This demonstrates that the beams are not phased after exiting the fiber and retracing their own path. This proves that a phase conjugate reflection of the pump beam is was not emitted from the fiber. Additionally, when the piezo electric stage is varied to induce a difference in path length, the interference from the central region of the beam profile, where the fringes arise from the mutual interference, was the only interference being affected. Figure 4.14 shows how by changing the path length in the order of wavelengths, the fringes can be aligned across the three regions. By using equation 4.1, it would be expected that with an SBS shift of $\sim 16\text{GHz}$ and a maximum piston correction error

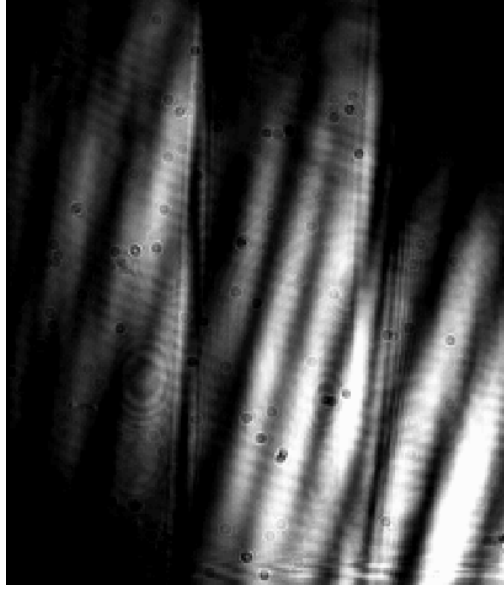


Figure 4.13: Data from the lateral shearing interferometer showing discontinuity throughout the three regions.

of 0.1 waves, the maximum path difference should be of 0.19cm when phasing of the two beam paths occurred. Experimentally, it was observed that the cyclic nature of this optical path length difference (OPD), $\delta \approx 0, 1, 2, \dots$, was manifested by moving the piezo-electric stage by $\sim 0.4\mu\text{m}$ or for an OPD of $\sim 0.8\mu\text{m}$. This demonstrates that phasing of the two beam paths is not achieved. Figure 4.15 shows that for small vibrations, the mutual fringes in the central region are washed out as a result of the small variation in path length needed to obtain continuity across the fringes from the three regions.

4.3 Conclusion

In this chapter the phasing properties of SBS were successfully investigated. The optical fiber was observed to act as beam cleanup device for a beam spatially divided into two equal halves. This result agrees with that obtained in chapter 3 where the Stokes beam traveling in the backward direction propagated in the LP_{01} mode. This demonstrated that regardless of the pump beam being coupled into the fiber, the resulting Stokes produced a Gaussian beam profile. This result only states that long

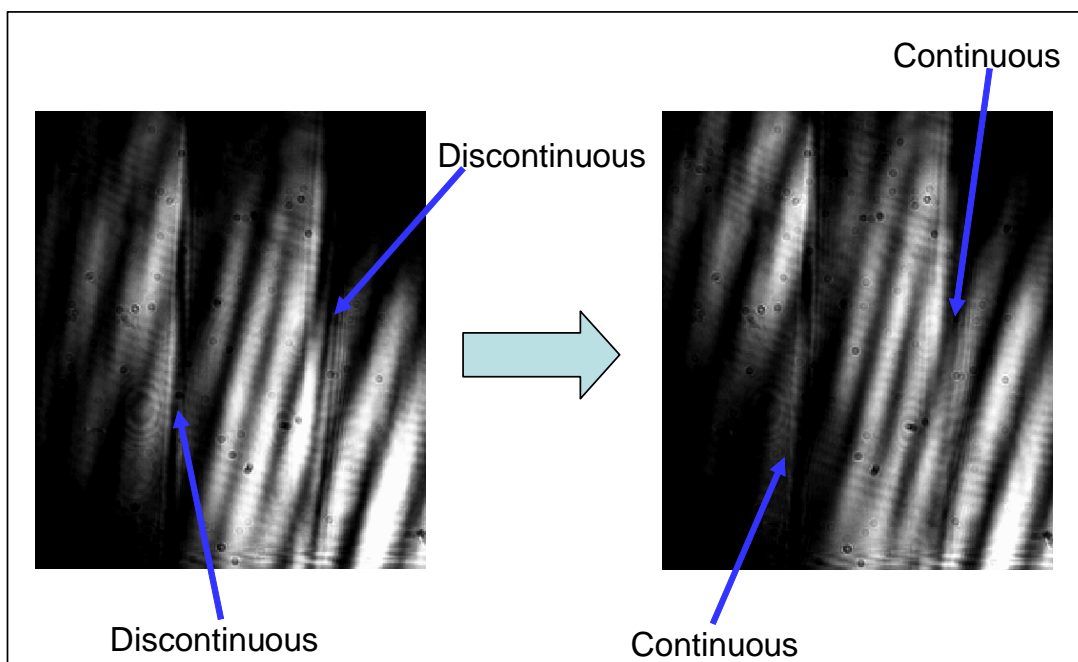


Figure 4.14: From discontinuity to continuity

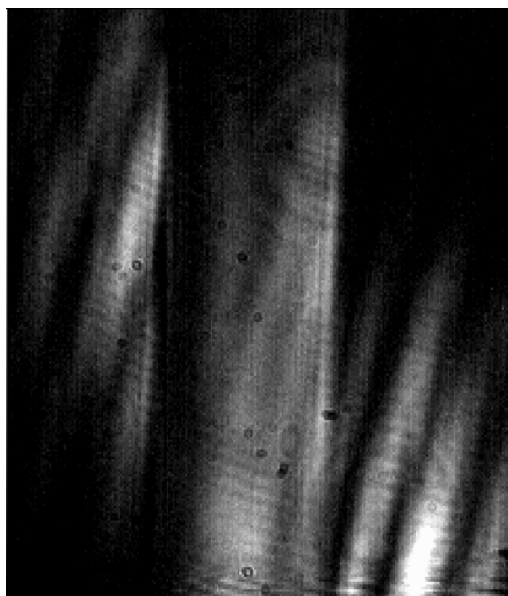


Figure 4.15: LSI data showing no fringes in the mutual interference region due to vibrational disturbance.

(\sim km) multimode fiber does not exhibit the properties of a real PCM. As shown by Willis, multimode fibers do in fact behave as a PCM but only for multimode fiber of lengths of approximately less than 10m.

Since the backward propagating Stokes beam is phased right after exiting the fiber, as it propagated through the two channel system once more, the beams became once again unphased. This also suggested that phase conjugation for the pump beam did not occur for long multimode fiber, otherwise the results from a two pass through the system would have exhibited a phased beam only after the two passes through the optical system.

V. Lateral Shearing Interferometer Testing

In this chapter, different configurations for the LSI will be presented as well as certain advantages and disadvantages that each device exhibited. There were a total of four built LSI systems for the sole purpose of studying the phase conjugation properties of SBS as originally developed by Moyer *et al.*⁵ The LSI systems consisted of a combination of 3 optical devices, which included wedges, optical flats, and microscope slides.

5.1 Two Microscope Slides

Microscope slides are the most easy and inexpensive way of building an LSI. A standard microscope slide is 75 x 25 mm and about 1.0 mm thick. They provide a versatile way of building an LSI because if mounted into a clamp, the microscope slide can be rotated and tilted in various ways allowing for a range of motion not possible with other optics. In the research performed by Willis, using two microscope slides proved to be a difficult diagnostic tool to understand. Nevertheless, the LSI displayed the continuities and/or discontinuities of the three interference regions, although the boundaries were not easily detectable.

During the course of our research, several problems were encountered when using two microscope slides as the LSI device for this experiment. The first one comes from the fact that microscope slides are not flat. This creates the problem of not being able to properly identify if the plates are parallel or not solely by observation.

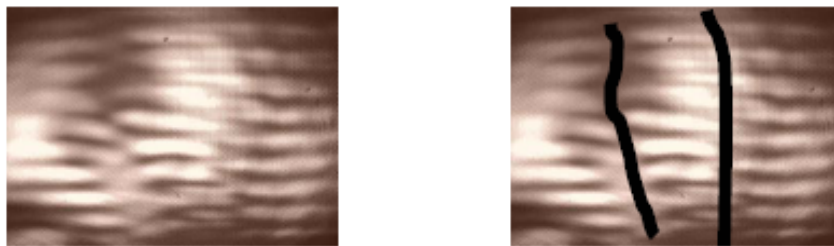


Figure 5.1: Interference pattern obtained from a LSI consisting of two microscope slides as performed by Willis.⁶ Notice that the boundary regions cannot be easily distinguished

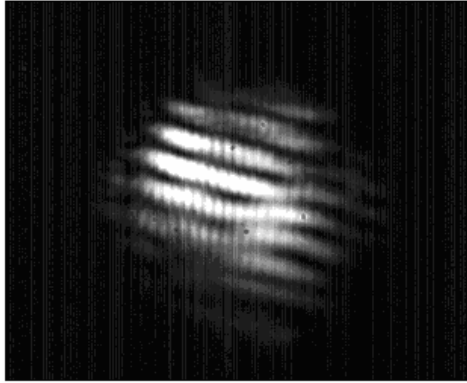


Figure 5.2: Interference pattern observed when a microscope slide was used to build the LSI. Notice that the boundaries between the regions are difficult to identified as this was the case in previous experiments.

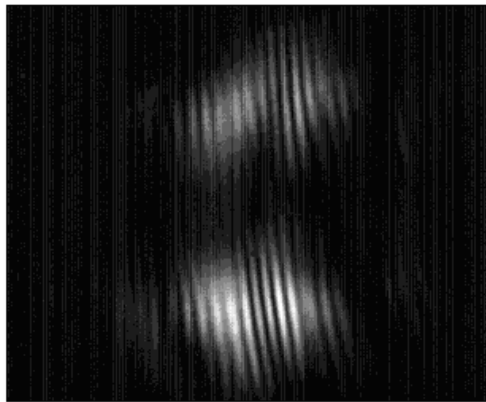


Figure 5.3: The two reflections of an LSI consisting of two microscope slides. Interference shown here may be developed as the beam is transmitted through the amplifier.

Another problem arises from the unevenness of the slides. It was observed that when the two reflections from the LSI were viewed separately, vertical interference fringes were visible. Figure 5.3 shows this interference pattern. These vertical fringes did not indicate beam phasing and added to the confusion of the already unclear data produced by this LSI. The fringes arise as a result of the overlap of the beams from the two reflections of the microscope slides surfaces. The two reflections from the same microscope slide cannot be separated. Additionally, when the two beams that were tiled next to one another were not sufficiently parallel to each other, the vertical fringes were observed to vary in resolution.

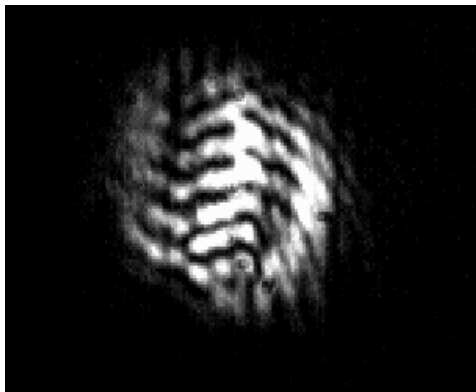


Figure 5.4: Interference pattern between the two optical flats as an LSI. The boundaries are not easily distinguishable.

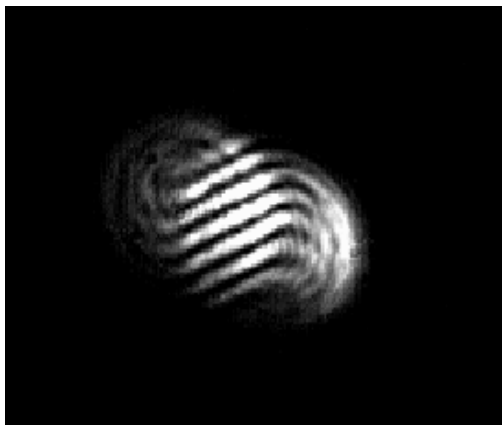


Figure 5.5: Interference of two reflections from a single optical flat was used as a LSI.

5.2 *Two Optical Flats*

Results obtained from the LSI composed of the two microscope slides suggested that a device consisting of a more even surface might improve the quality of the LSI beam profiles. By using the same principles once again, two optical flats of 25.4 mm in diameter and 4.2 mm of thickness were aligned. The results are shown in figure 5.4. The data collected from two LSI showed a significant improvement to that of the microscope slides. First of all, a better separation of the fringes can be detected, allowing the user to somewhat determine the boundaries of each region.

When the two reflections from the LSI were separated it was observed that both of these optics showed an interference pattern. This was as a consequence of

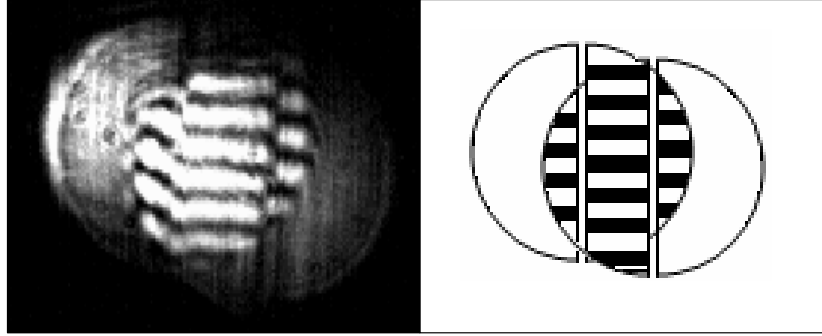


Figure 5.6: LSI interference using an optical flat.

the reflections from the two surfaces of a single optical flat. It was then that the idea to use a single optical flat as the LSI unfolded.

5.3 *Single Optical Flat*

By testing the viability of using two optical flats as an LSI, it was discovered that a single optic would give better results than the combination of two of them. Instead of using two surfaces from two different optics, it was shown that a single optical flat was capable of exhibiting very clearly defined data. As shown in picture 4.6 from chapter 4, the three regions consisting of self interference of beam 1,2 and mutual interference are clearly visible. Notice that the data obtained with this LSI shows in detail the boundaries of each region.

By switching from using two optical flats to just one, it is possible to eliminate unwanted reflections, discarding the potential of not properly ignoring the reflections caused by the outer surfaces. Figure 5.5 shows the data obtained by reflecting a test reference beam into the LSI without aligning the optical flat. Notice that the fringes across the two reflections are inclined by a certain degree. By simply rotating the optic, the fringes also rotate in such a way that the fringes are perfectly horizontal. In this research, it was found that the degree of flatness of the optical flats in used were not as negligible as it was anticipated. The surfaces where not parallel with respect to one another which would be expected from an optical flat. This meant that it was necessary to determine by trial and error the location where the incident

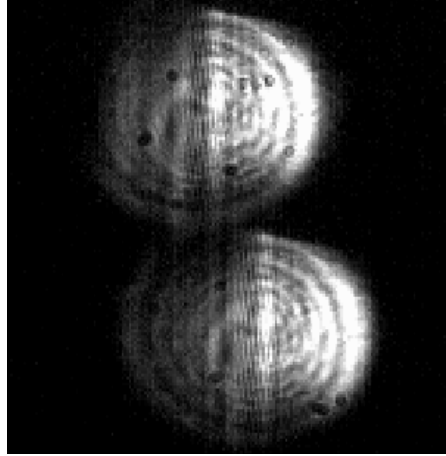


Figure 5.7: LSI built with two wedges.

beam on the LSI proved to yield better results. This usually consisted of rotating the optic and changing the angle between the incident and the reflected beam in such a way to obtain an angle that was as small as possible, which usually resulted in greater separation of the beams reflected from the surfaces of the optical flats.

The best advantage provided by the optical flat is that because of the fixed distance between the two surfaces, it was possible to readjust the interference pattern in a matter of seconds and each time obtaining a result that is not a function of the plate separation. The optical flat worked just as if the LSI consisted of two optical pieces built into one. In the experiment developed by Moyer *et al*, two wedges were used such that the two reflection from each wedge could be separated by a determined distance to prevent them from combining with the inner reflection and as a means to obtain an additional beam for diagnostics. The wedges were also considered for this experiment and are addressed in the next section.

5.4 Two Optical Wedges

As stated before, the original LSI as described by Moyer consisted on the use of two wedges. The experimental data obtained during his investigation showed clearly defined boundary regions. This approach seemed to be the most effective device in obtaining detailed information about the interference fringes from the LSI. The only

disadvantage is that the plates need to be aligned and the plate separation had to be kept constant manually. An advantage of using wedges is that the interference pattern can be split, rotated and adjusted in any way by just adjusting the distance and orientation between the plates. During the course of this research, a limited amount of wedges were available and this approach could not be implemented.

VI. Conclusion and Recommendations for Future Work

6.1 Conclusion

In this research the beam cleanup and phasing properties of a long multimode optical fiber as a PCM were investigated and characterized. Two different experiments that complemented each other were studied in this thesis. The first part of this research consisted in coupling an aberrated beam into a multimode fiber. By doing so, it was demonstrated that the backward moving Stokes is the fundamental fiber mode LP_{01} as a consequence of SBS in the medium regardless of the pump beam spatial distribution.

The second part consisted of building two separate optical paths for each side of the beam. These paths were built using right angle prisms to spatially divide a beam into two equal semicircles. Each beam traveled its own path toward the optical fiber. One path remained fixed while the other contained an embedded movable stage by which the optical path length could be increased or decreased on the order of a few wavelengths. This difference in path length created a phase delay or piston error between the beams.

To properly characterize the piston error and the phase conjugation properties of SBS in this fiber, a LSI was utilized. Generally, it consists of two parallel plates that create an interference pattern from the two reflections of the two inside surfaces of the plates. The first spatial distribution analyzed was the Stokes beam just after exiting the fiber as it traveled in the backward direction. When observed using the LSI as the diagnostic tool, it was revealed that the left and right side of the beam phased. Additionally, it was noted that the beam had a Gaussian-like spatial distribution which was predicted by the first part of this research when the beam cleanup properties were studied.

The two sides of the beam then traveled back through their individual paths and reached the second LSI in the system. The LSI data revealed that the interference fringes across the three regions were not continuous thus the two beams were not phased. The interference fringes produced by the mutual interference of the beams

from both paths could be varied as the movable stage was displaced. By adjusting the path, variations in the relative phase delay between the two beams were created and observed with the LSI as the shifting of fringes in the central region.

6.2 Recommendations

Several ideas concerning the work developed in this research arise as the outcome of the results obtained. Because phase conjugation of a pump beam for a long length of multimode fiber has been disproved, particular questions remained. This research determined that phase conjugation does not occur in long multimode fiber, in this case of 4.6km, then what is the maximum length at which these fibers stop behaving as a PCM? As seen earlier, the fiber length at which the Stokes beam changes from a conjugate beam to an LP_{01} is not clear.

Research should be developed concerning the different lengths of fiber suggested by papers for a multimode fiber to behave as a PCM. By doing so, an investigation of PCM in multimode fiber can be implemented beginning with the largest and smallest value obtained from several investigations. From this absolute length difference, the gap could be reduced by reducing the limits at which phase conjugation shifts to beam cleanup. The method could be analogous to implementing the bisection method for a given range. In this way, the value could be approximated experimentally in order to at least obtain a more confined range at which this shift is believed to occur.

Concerning the future of this research, an approach to develop this concept further would involved implementing the use of fiber amplifiers in both paths. The LSI configuration should remain fairly similar such that each boundary region can be easily determined. The acquisition of very precise mounts would guarantee that the Stokes beam observed from either LSI could develop fairly accurate spatial beam profiles. In this research, several problems occurred with forcing each side of the Stokes beam to retrace its own path individually.

Bibliography

1. <http://inventors.about.com/od/lstartinventions/a/laser.htm> - History of Lasers, Jan 2007.
2. <http://www.coherent.com/Applications/> - Coherent Inc. - Laser Applications, Jan 2007.
3. <http://www.cbsnews.com/stories/2003/10/20/tech/main578998.shtml> - Laser Weapons In U.S. Sights, CBS News, Jan 2007.
4. <http://www.globalsecurity.org/military/systems/aircraft/systems/atl.htm> - Global Security, Jan 2007.
5. R. H. Moyer, M. Valley, and M.C. Cimolino, "Beam combination through stimulated Brillouin scattering," J. Opt. Soc. Am. B, vol. 5, pp. 2473-2489, 1988.
6. Willis, Shawn, Phasing a Dual Optical Path System Using an Optical Fiber and a Phase Conjugate Mirror, MS Thesis, AFIT/GAP/ENP/03-06, School of Engineering, Air Force Institute of Technology, Wright-Patterson AFB, 2003 (ADA412678).
7. B. Ya. Zel'dovich, V.I. Popovichev, V.V. Ragul'skii, and F.S. Faisullov, "Connection between the wave fronts of the reflected and exiting light in stimulated Mandel'shtam-Brillouin scattering," Pis'ma Zh. Eksp. Teor. Fiz. 15, 160-164 (1972) [JTEP Lett. 15, 109-113 (1972)].
8. Rodgers, B. C., T. H. Russell, and W. B. Roh, "Laser beam combining and cleanup by stimulated Brillouin scattering in a multimode optical fiber," Opt. Lett., 24, 1124-1126, 1999.
9. Russell, T. H., W. B. Roh, and J. R. Marciante, "Incoherent beam combining using stimulated brillouin scatterring in multimode fibers." Opt. Lett., 8, 246-254, 2001
10. Grime, Brent W., Multiple Channel Laser Beam Combination and Phasing Using Stimulated Brillouin Scattering in Optical Fibers., PhD Dissertation, AFIT/DS/ENP/06-01, School of Engineering, Air Force Institute of Technology, Wright-Patterson AFB, 2002 (ADA398033).
11. W. Ubachs, Nonlinear Optics Lecture Notes, Laser Centre Vrije Universiteit Amsterdam, <http://www.nat.vu.nl/126wimu/NLO-2001.pdf>, 2001.
12. Saleh, B. E., Teich, M. C., Fundamentals of photonics, Teich, Malvin Carl. New York : Wiley, 1991.
13. Agrawal, Govind. P., Nonlinear Optics, 3rd ed., San Diego. Academic Press, 2001
14. R. W. Boyd, Nonlinear Optics, San Diego: Academic Press Inc., 1992.
15. E. Hecht, Optics, Addison-Wesley, Reading, Massachusetts, 1998.

16. Bruesselbach, H., "Beam cleanup using stimulated Brillouin scattering in multi-mode fibers," Conf. of Las. and Elec. Opt.,11,424,1993.
17. A. Mocofanescu and K.D. Shaw, Stimulated Brillouin scattering phase conjugating properties of long multimode optical fibers, Opt. Comm, vol. 266, no. 1, 307-316, Oct 2006.
18. M.J. Damzen, V.I. Vlad, V. Bambin, A. Mocofanescu, Stimulated Brillouin Scattering- Fundamentals and Applications, Institute of Physics Publishing, Bristol, UK, 2003.
19. Basov, N. G., I. G. Zubanrev, A. B. Mironov, and S. I. Mikhailov, and A.Y. Pokulov, "Laser interferometry with wavefront-reversing mirrors,"Sov. Phys. JETP, 52, 847-851, 1990.
20. S. Sternklar, D. Chomsky, S. Jackel, and A. Zigler, "Misalignment sensitivity of beam combining by stimulated Brillouin scattering," Opt. Lett., vol. 15, no. 9, pp. 469-470, May 1990.
21. M. Gower, D. Proch, Optical Phase Conjugation, Berlin: Springer-Verlag, pp. 74-96, 1994.
22. B. Ya. Zel'dovich, V. V. Shkunov: Kvant. Electron. 4, 1090-1098, 1977 [Sov. J. Quantum Electron. 4, 610 (1977)].

Vita

Second Lieutenant Omar Gamboa graduated from Dr. Santiago Veve Calzada High School in Fajardo, Puerto Rico. In August 2000, he attended the University of Puerto Rico - Mayaguez Campus and later transferred to the University of Puerto Rico - Rio Piedras Campus, where he graduated with a Bachelor of Science degree in Physics in May 2005. There, he was commissioned through the Detachment 755 AFROTC. His first commissioned assignment, in August 2005, was at the Graduate School of Engineering and Management, Air Force Institute of Technology, Wright-Patterson AFB, Ohio where he pursued a Master of Science degree in Applied Physics.

REPORT DOCUMENTATION PAGE				<i>Form Approved OMB No. 0704-0188</i>	
<small>The public reporting burden for this collection of information is estimated to average 1 hour per response, including the time for reviewing instructions, searching existing data sources, gathering and maintaining the data needed, and completing and reviewing the collection of information. Send comments regarding this burden estimate or any other aspect of this collection of information, including suggestions for reducing the burden, to the Department of Defense, Executive Services and Communications Directorate (0704-0188). Respondents should be aware that notwithstanding any other provision of law, no person shall be subject to any penalty for failing to comply with a collection of information if it does not display a currently valid OMB control number.</small>					
PLEASE DO NOT RETURN YOUR FORM TO THE ABOVE ORGANIZATION.					
1. REPORT DATE (DD-MM-YYYY)		2. REPORT TYPE		3. DATES COVERED (From - To)	
4. TITLE AND SUBTITLE				5a. CONTRACT NUMBER	
				5b. GRANT NUMBER	
				5c. PROGRAM ELEMENT NUMBER	
6. AUTHOR(S)				5d. PROJECT NUMBER	
				5e. TASK NUMBER	
				5f. WORK UNIT NUMBER	
7. PERFORMING ORGANIZATION NAME(S) AND ADDRESS(ES)				8. PERFORMING ORGANIZATION REPORT NUMBER	
9. SPONSORING/MONITORING AGENCY NAME(S) AND ADDRESS(ES)				10. SPONSOR/MONITOR'S ACRONYM(S)	
				11. SPONSOR/MONITOR'S REPORT NUMBER(S)	
12. DISTRIBUTION/AVAILABILITY STATEMENT					
13. SUPPLEMENTARY NOTES					
14. ABSTRACT					
15. SUBJECT TERMS					
16. SECURITY CLASSIFICATION OF:			17. LIMITATION OF ABSTRACT	18. NUMBER OF PAGES	19a. NAME OF RESPONSIBLE PERSON
a. REPORT	b. ABSTRACT	c. THIS PAGE			19b. TELEPHONE NUMBER (Include area code)